Flow patterns on an inkjet nozzle plate

Beulen, B.W.A.M.M.

Award date:
2005

Flow patterns on an inkjet nozzle plate

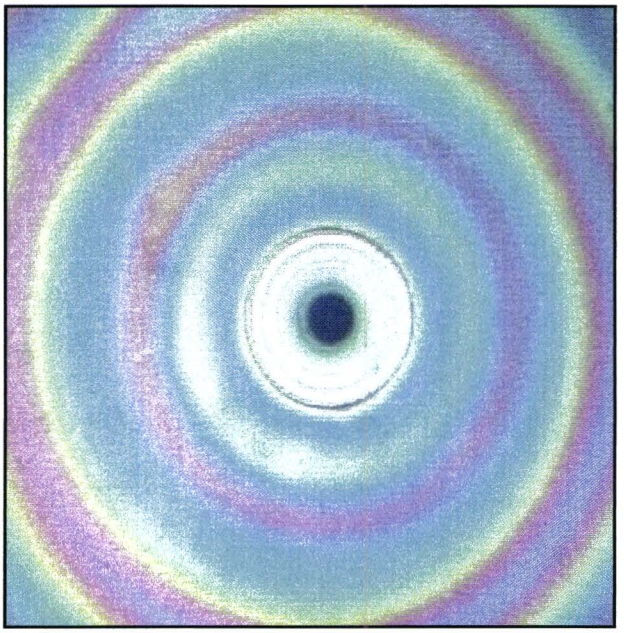

B.W.A.M.M. Beulen
Applied Physics
TU/e Eindhoven

TU/e:
Prof. Dr. Ir. M.E.H. van Dongen

Océ:
Ir. H. Reinten

TU/e technische universiteit eindhoven

océ

Summary

At Océ Research & Development research is performed on piezo inkjet heads. By deforming an inkchannel using a piezo actuator an acoustic pressure field is created in the inkchannel. The acoustic waves result in a strong acceleration of the fluid in the nozzle, such that a droplet is generated.

During previous research, it is often observed that after a period of jetting, a thin ink layer is formed on the nozzle plate. The presence of this ink layer is often linked with instability:

1. When dirt particles are caught in the ink layer, transport in the ink layer can cause them to reach the nozzle. At the nozzle these particles can disturb the drop formation, which can cause air bubbles to be formed. These air bubbles can cause nozzle failure by disturbing the pressure waves in the ink channel.
2. The ink layer itself, at a critical layer thickness, can cause air bubbles due to cavity collapse. The air bubbles can subsequently cause nozzle failure by disturbing the pressure waves in the ink channel.

In this research the transport and flow mechanisms in the ink layer on the nozzle plate are determined by applying tracer particles to the ink and using Particle Tracking Velocimetry (PTV) to determine the velocities in the ink layer.

It is shown that under practical print conditions, there is always an ink layer present on the nozzle plate of the checked printheads. This is caused by the small contact angle ($\theta < 20°$) of the ink.

Jetting actuation pulses cause sink/source-like flow fields on the nozzle plate. The driving forces behind the flow fields on the nozzle plate are surface tension and in case of jetting friction with airflow induced by the jet of droplets.
Analysis shows that the flow in the ink layer on the nozzle plate can be described by 2D potential flow. Small deviations can occur due to non uniform layer thickness.

Experiments have shown a flow of ink towards jetting nozzles. This transport can cause dirt particles, which are caught in the ink layer on the nozzle plate, to reach the nozzle and cause instability.

Experiments on a nozzle with initially dry surroundings show that the nozzle leaks at frequencies below 13 kHz. At higher frequencies the surroundings of the nozzle remain dry.

Experiments with non-jetting nozzles have shown that these nozzles generally show leakage when actuated at voltages above 4V. At a voltage just below the transition voltage from non-jetting to jetting, a transition to a dipole-like field occurs.
The mechanism behind this dipole remains unknown, but it is expected that non-uniform wetting conditions near the nozzle cause an asymmetrical movement of the meniscus.

Preface

This research has been performed at Océ Technologies B.V. It is the master thesis for my study Applied Physics at the TU/e. I worked at Research and Development on a printhead for hotmelt ink using piezo technology.

I would like to thank my supervisor from Océ, Hans Reinten for his help and support. Special thanks go out to Jos de Jong and Marc van den Berg, for their help on the experimental aspects of this research, and to Roger Jeurissen, for the valuable discussions on various theoretical aspects.

I would also like to thank Rini van Dongen, my supervisor from the TU/e for his help and support.

It was a valuable experience to do research at Océ. I acquired a good insight in working in an R&D department of a multi-national.

Venlo, April 2005

Bart Beulen

List of Symbols

Physical Properties:

ν	Kinematic viscosity (m^2s^{-1})
μ	Dynamic viscosity ($kgm^{-1}s^{-1}$)
ρ	Density (kgm^{-3})
σ	Surface tension (Nm^{-1})

Subscripts *l* and *a* respectively denote ink and air properties.

Jetting Properties:

v_{drop}	Droplet speed (ms^{-1})
V_{drop}	Droplet volume (m^3)
f_{DOD}	Jet frequency (s^{-1})
U_{DOD}	Amplitude jet pulse (V)

Table of contents

1. Introduction

At Océ Research & Development research is performed on piezo inkjet heads. By deforming an inkchannel using a piezo actuator an acoustic pressure field is created in the inkchannel. The acoustic waves result in a strong acceleration of the fluid in the nozzle, such that a droplet is generated.

The droplets have to meet high requirements in speed, volume and diameter. One of the most important parts of the jetting process is its stability. Billions of droplets have to be jetted faultlessly. There are, however, a lot of factors that can disturb the jetting process.
One possible failure mechanism is an air bubble in the nozzle that disturbs the pressure waves in the ink channel. Research has indicated that dirt particles can cause air bubbles.

During previous research, it is often observed that after a period of jetting, a thin ink layer is formed on the nozzle plate (figure 1.1). First estimates for the horizontal dimensions of the ink film are in the order of 10^{-3} m and for the thickness in the order of 10^{-5} m.
The ink layer is observed both on printheads that are placed in a stationary printhead test setup and printheads that are placed in a moving carriage in a total printer setup.

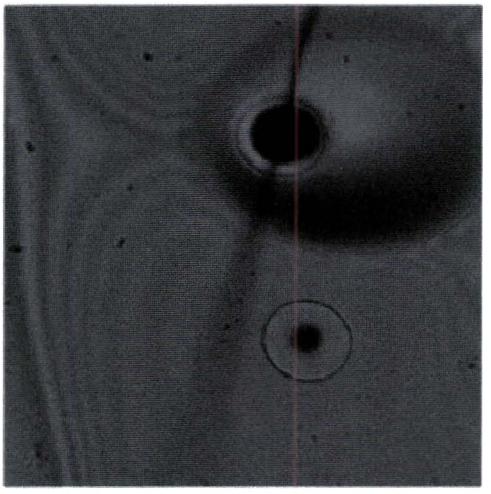

Figure 1.1: During jetting a thin ink film is formed near the nozzle on the nozzle plate [JON03]

The presence of this ink layer is often linked with instability:

1 When dirt particles are caught in the ink layer, transport in the ink layer can cause them to reach the nozzle. At the nozzle these particles can disturb the drop formation, which can cause air bubbles to be formed. These air bubbles can cause nozzle failure [MVDB].

1. The ink layer itself, at a critical layer thickness, can cause air bubbles due to cavity collapse. The air bubbles can subsequently cause nozzle failure [JON03].

The main purpose of this research is to get a better understanding of the transport and flow mechanisms in the ink layer.

2. Approach

Before describing the experiments on the ink layer on the nozzle plate, a list of possible forces, mechanisms and parameters influencing the ink layer properties and ink layer behaviour on the nozzle plate is discussed. This is followed by an outline of the thesis.

2.1 Factors affecting ink layer behaviour

The wetting properties of the ink on the nozzle plate primarily determines the behaviour of the ink on the nozzle plate.
If the molecules of the ink have a stronger attraction to the molecules of the nozzle plate surface than to each other (the adhesive forces are stronger than the cohesive forces), wetting of the nozzle plate occurs: an ink film is formed.
Alternately, if the ink molecules are more stronger attracted to each other than to the molecules of the nozzle plate surface (the cohesive forces are stronger than the adhesive forces), then the ink does not wet the nozzle plate surface: the ink forms droplets on the nozzle plate.

The surface wetting characteristics of the ink on the nozzle plate can be expressed in the contact angle, θ (figure 2.1).

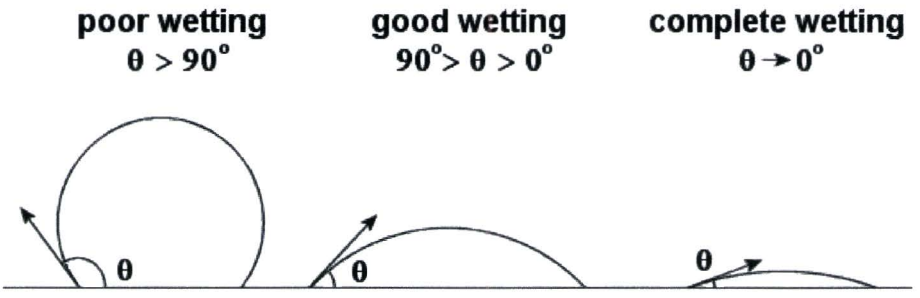

Figure 2.1: the contact angle determines the wetting behaviour of the ink on the nozzle plate.

It is known that the contact angle of the ink on the nozzle plate is less than 20 degrees. This indicates that the ink will form an ink layer on the nozzle plate.
In the next sections the forces, mechanisms and parameters acting on the ink layer on the nozzle plate are discussed.

2.1.1 Forces

The forces acting on the ink layer on the nozzle plate are:

1. **Surface tension**
   In the case of a non-uniform layer thickness, surface tension causes a pressure gradient, which causes the ink layer to smoothen.

2. **Gravity**
   The nozzle plate is the bottom side of the printhead. Gravity causes pressure gradients, which drive ink towards spots with the largest layer thickness. This can cause the formation of a drop.

3. **Static forces**
   A negative average pressure (compared to ambient) is applied to the nozzle. Together with the capillary effect this can cause ink on the nozzle plate to move towards the nozzle.

4. **Electrostatics**
   At the edges of the nozzle plate another part of the print head is glued to it. It is observed that the ink layer always stays at a certain distance from these edges. This could be due to electrostatic repulsion between the ink and the glue.

5. **Carriage movement**
   In a total printer setup the ink layer on the printhead experiences large forces due to the accelleration of the carriage. This results in a pressure gradient, which influences the behaviour of the ink on the nozzle plate.

2.1.2 Mechanisms

Possible mechanisms influencing the behaviour of the ink layer on the nozzle plate are:

1. **Jetting**
   Jetting causes the nozzle to act as a pump [HEI98]. Not all the ink pumped will go into droplets, some leakage can occur. This depends on the channel acoustics and nozzle shape.

2. **Vibration of the nozzle plate**
   Due to the actuation of the piezo the nozzle plate can vibrate, forming nodes and anti-nodes of displacement. It is expected that this vibration is on nanometer scale and cannot influence the behaviour of the ink on the nozzle plate.

3. **Thermal**
   The temperature distribution on the nozzle plate can be non-uniform. A temperature dependent surface tension can give rise to the Marangoni effect. This can cause ink flow on the nozzle plate.

4. **Acoustic streaming**
   Acoustic waves can originate from the nozzle. Travelling through the ink layer these waves can cause ink flow.

5. **Capillary waves**
   The movement of the ink layer near the nozzle can cause capillary waves, which subsequently can cause ink flow on the nozzle plate.

2.1.3 Parameters

The following parameters can be used to influence the behaviour of the ink layer on the nozzle plate.

1. **Surface properties**
   The properties of the surface determine the wetting behaviour of the ink on the nozzle plate. The roughness of the nozzle plate surface can be used to influence the wetting properties of the ink on the nozzle plate.

2. **Ink**
   The properties of the ink (density, viscosity and surface tension) will be used to influence the behaviour of the ink layer on the nozzle plate.

3. **Jetting**
   The flows induced by the nozzle probably depend on the properties (amplitude, frequency, timing) of the actuation pulse. Also the pattern of active nozzles and the prehistory of active nozzles is important.

2.2 Outline

In this research it is tried to visualise the flows on the nozzle plate using tracer particles and to determine which of the forces and mechanisms mentioned in 2.1 are responsible for the flows observed.

The thesis starts with an overview of the existing knowledge of the printhead and the drop formation process in chapter 3

In chapter 4 the theoretical aspects of this research are discussed. The chapter starts with a description of the ink flow on the nozzle plate in terms of dimensionless groups. This shows that the ink flow on the nozzle plate can be described by creeping motion (section 4.2). From the Hele-Shaw analogy it follows that the flow on the nozzle plate can approximately be described using 2D potential flow (section 4.3).
Section (4.4) discusses the spreading of an ink layer under influence of the surface tension and gravity.
The chapter ends with a short description of acoustic streaming and a discussion on the different types of flow fields that acoustic streaming can cause on the nozzle plate.

In chapter 5 the experimental methods of this research are discussed. The chapter starts with a description of the experimental setup. This setup is used to visualise the movement of the ink layer using Particle Tracking Velocimetry (PTV). The chapter ends with a short description of the PTV script and an overview of the measuring method.

In chapter 6 the experimental results are discussed. Experiments are performed using jetting and non-jetting actuation pulses. Both show very different flow fields on the nozzle. The chapter ends with a discussion on the different mechanisms that can cause these flow fields.

In chapter 7 the flow fields, depending on the frequency and amplitude of the actuation, are mapped.

The measurements in chapter 6 and 7 indicate that the movement of the ink layer on the nozzle plate is influenced by the airflow induced by the jet of droplets. In chapter 8 experiments are discussed which prove that the jet of droplets causes an airflow which is strong enough to influence the movement of the ink layer on the nozzle plate. The chapter ends with some sections on modelling the airflow.

Chapter 9 discusses the measurements performed using the Speckle Interferometer setup. This setup is used to check whether there are vibrations present on the nozzle plate.

The thesis ends with the conclusions and discussion in chapter 10. In this chapter it is tried to link the observed flow fields on the nozzle plate to the different mechanisms causing nozzle failure.

3. The printhead

3.1 Printhead overview

One of the present fields of research at Océ Research & Development is inkjet technology. Worldwide two major drop-on-demand technologies can be distinguished: thermal and piezo technology.
This research is performed on a printhead using piezo technology. By deforming an inkchannel by a piezo actuator an acoustic pressure field in the inkchannel is created. The acoustic waves result in a strong acceleration of the fluid in the nozzle, such that a droplet is generated. Each channel has its own piezo element, which can be actuated separately. This technology is called drop-on-demand (DOD).
Hot melt ink is used in this head. Hot melt ink is a solid at room temperature but a liquid at the operating temperature of the head.

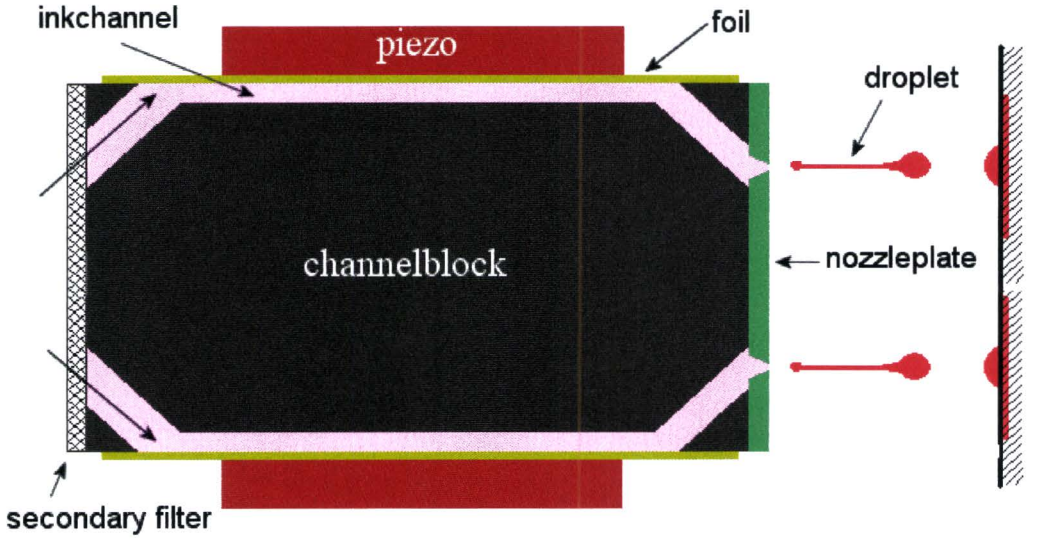

Figure 3.1: an overview of the channelblock

The printhead consists of two arrays of inkchannels. At one end the inkchannels have small nozzles and at the other sides they are connected to an ink reservoir. An overview is given in figure 3.1.
There is a filter in front of the inkchannels to prevent small dirt particles from entering the inkchannel. To prevent ink from leaking from the nozzles a negative (compared to ambient) pressure is maintained above the filter. The ink then moves through the inkchannel, which is deformed by the piezo actuator. A foil is placed between the actuator and the channel to prevent ink from leaking between the piezo and the channelblock. At the nozzles the ink droplets are formed and transferred to the medium.

Figure 3.2 clearly shows the different fingers, which the piezo actuator consists of. As already mentioned these fingers can be actuated separately. This makes it possible to control every droplet individually.

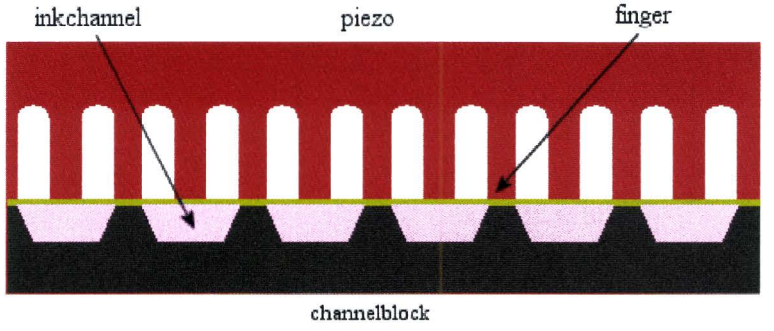

Figure 3.2: An overview of the different inkchannels

3.2 Drop formation

In the piezo inkjet printhead in this research, actuating a piezo element leads to the deformation of an inkchannel. This results in a pressure wave in the inkchannel. By tuning the actuation pulse to the resonance frequency of the channel it is possible to jet droplets from the nozzle.

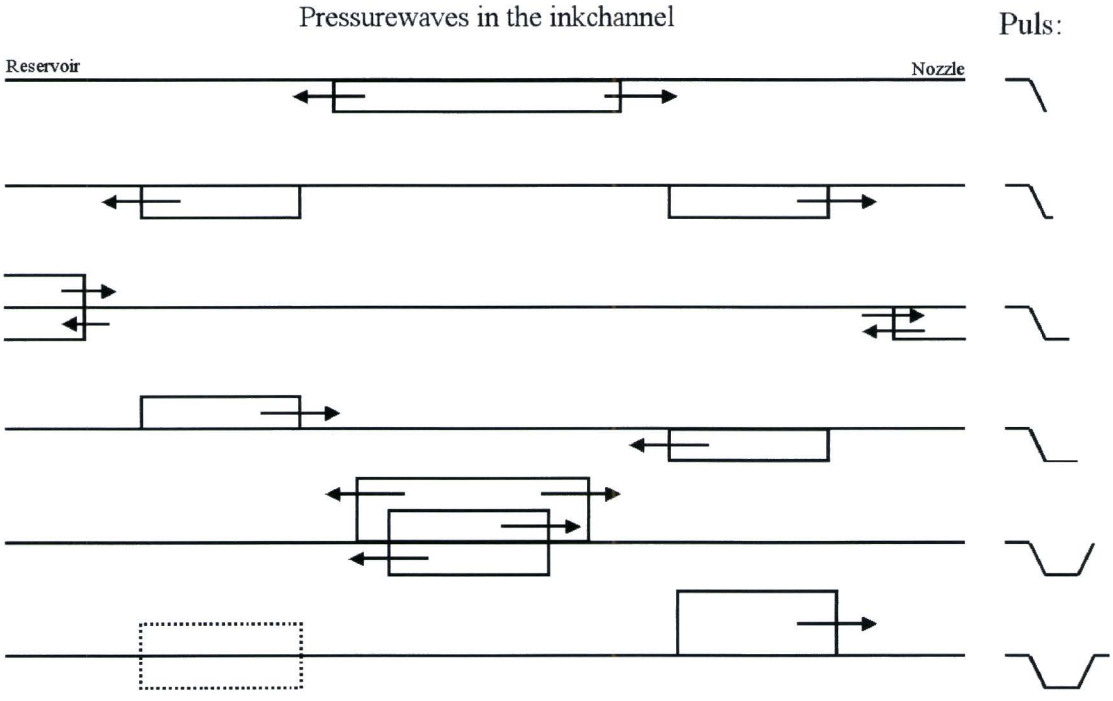

Figure 3.3: schematic representation of the pressure waves in the inkchannel during actuation

In general a trapezium shaped pulse is used to actuate the piezo. This pulse is defined by the rise time, the high time and the descend time. For example, a pulse with a rise time of 5 microseconds, a high time of 5 microseconds and a descend time of 3 microseconds is denoted as a 553 pulse.

At the first edge of the trapezium shaped pulse the finger is contracted, which leads to expansion of the inkchannel, creating negative pressure waves. One pressure wave travels towards the nozzle and one wave travels towards the ink reservoir.
The reflection between ink channel and ink reservoir is approximately open, reversing the sign of the pressure wave. The reflection at the nozzle is much more complex. Both inertia and flow resistance in the nozzle play an important role. When the nozzle plate can be taken as approximately closed the sign of the incident and reflected pressure waves are the same.
After the reflections there is a negative pressure wave travelling from the nozzle towards the reservoir and a positive pressure wave travelling from the reservoir towards the nozzle. A schematic representation of the pressure waves in the inkchannel is presented in figure 3.3.

When both pressure waves are again located at the centre of the channel, the piezo element is expanded again. This results in a positive pressure wave in the channel. The positive pressure wave amplifies the positive pressure wave that was already travelling to the nozzle, which leads to the jetting of a droplet. The negative pressure wave moving towards the reservoir is cancelled by the positive pressure wave travelling in the same direction. This is important because the acoustic waves have to be damped as much as possible before the next actuation begins.

When an air bubble is present in the ink channel, it disturbs the pressure fields in the ink channel. This can cause a deviation in the droplet properties. Figure 3.4 shows the droplet formation without (left) and with (right) an air bubble present in the ink channel.

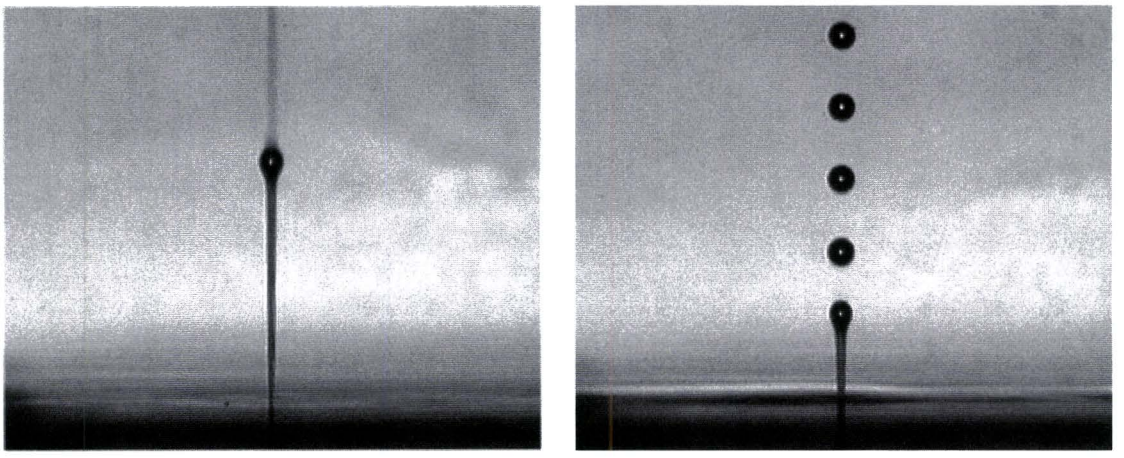

Figure 3.4: The drop formation at 20 kHz is visualised using stroboscopic lighting: a decrease in drop-to-drop distance is equivalent to a decrease in droplet speed. At the left the standard drop formation is shown. The image at the right shows the drop formation when an air bubble is present in the ink channel. The decrease in jet speed caused by the presence of the air bubble is clearly visible.

In this case the air bubble causes a decrease in jet speed. In the worst case however, a bubble can also cause nozzle failure: no droplet is formed.

4. Theoretical aspects

In this chapter, first a description of the flow on the nozzle plate in terms of dimensionless groups is given. Second a theory for describing the flows on the nozzle plate is formulated.
The chapter ends with a short description of acoustic streaming and a discussion how acoustic streaming could occur on the nozzle plate.

4.1 Flow characteristics

A dimensionless group is a quantity, which describes a certain physical system. For the experimenter, different systems, which share the same description in terms of dimensionless groups, are equivalent.

The following dimensionless groups describe the flow on the nozzle plate:

- Reynolds number
- Bond number
- Capillary number

A characteristic layer thickness H, a characteristic velocity V and a curvature radius R (figure 4.1) can describe the ink layer on the nozzle plate.

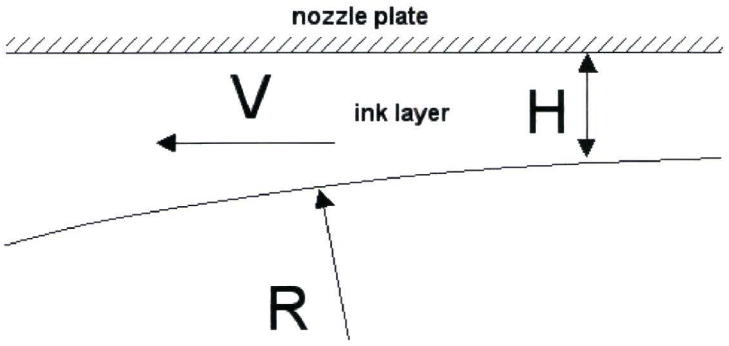

Figure 4.1: The ink layer can be described by the parameters R and H.

4.1.1 Reynolds number

The most important dimensionless group is the Reynolds number, which is used to determine whether the inertial or viscous forces are dominant. The Reynolds number is defined as the ratio between the inertial force and the viscous force:

$$\mathrm{Re} = \frac{\rho V H}{\mu}, \tag{4.1}$$

where ρ is the density of the fluid, μ is the dynamic viscosity and H and V are respectively the characteristic layer thickness and velocity.

4.1.2 Bond number

The Bond number is the ratio between gravity and surface tension and is often used in the motion of bubbles and droplets. In this specific case the Bond number can be defined as:

$$Bo \approx \frac{p_{gravity}}{p_\sigma} = \frac{g\Delta\rho H}{\sigma / R} = \frac{g\Delta\rho}{\sigma} HR, \tag{4.2}$$

where g is the gravitational acceleration, $\Delta\rho$ the difference in density of the fluid and the surrounding gas, H the characteristic layer thickness, R the curvature radius and σ the surface tension.

4.1.3 Capillary number

The capillary number is used to determine whether the viscous force or the surface tension force is dominant. The capillary number is defined as:

$$Ca = \frac{\mu V}{\sigma} \frac{R}{H}, \tag{4.4}$$

where μ is the dynamic viscosity, σ the surface tension, V the characteristic velocity scale, H the characteristic layer thickness and R the curvature radius.

4.1.4 Overview

Table 4.1 gives an overview of the ink properties and the characteristic length and velocity scales.

Table 4.1: Overview of the dimensionless groups.

Ink properties:	Value
Density ρ	1090 kgm^{-3}
Surface tension σ	$32 \cdot 10^{-3}$ Nm^{-1}
Dynamic viscosity μ	0,01 $kgm^{-1}s^{-1}$
Temperature T	130°C
Contact angle θ	less than 20°
Characteristic velocity, $V \approx 1 \cdot 10^{-3}$ ms^{-1}.	
Characteristic layer thickness, $H \approx 1 \cdot 10^{-5}$m.	

From the Reynolds number ($O(10^{-2})$) it can be concluded that the viscous forces are large compared to inertia.
The value of the Bond and the Capillary number depend on the local curvature and thickness of the ink layer. For a large curvature (small R) and small ink layer thickness, the surface tension dominates gravity and viscosity, while for small curvature (large R) and large ink layer thickness gravity dominates the surface tension and viscosity.

4.2 Creeping flow

For small Reynolds numbers (Re<<1) the inertia terms in the Navier Stokes equations can be neglected. The x and y directions are along the nozzle plate, the z direction is perpendicular to the nozzle plate. The Navier Stokes equations and the equation of continuity assume the form:

$$grad(p) = \mu \nabla^2 \vec{v} \tag{4.5}$$

$$div(\vec{v}) = 0\,. \tag{4.6}$$

Assume that the horizontal dimension of the layer are much larger than the vertical dimensions of the layer and assume that *w=0.* Equation (4.5) reduces to:

$$\frac{\partial p}{\partial x} = \mu\left(\frac{\partial^2 u}{\partial z^2}\right) \tag{4.7}$$

$$\frac{\partial p}{\partial y} = \mu\left(\frac{\partial^2 v}{\partial z^2}\right) \tag{4.8}$$

Assume a layer thickness, *h*, in the surroundings of the nozzle. The continuity of mass (for constant density), for a creeping flow may be formulated as:

$$\frac{\partial h}{\partial t} + \nabla_H \cdot (h\bar{\bar{v}}) = 0\,, \text{ with } \nabla_H = (\frac{\partial}{\partial x}, \frac{\partial}{\partial y}) \tag{4.9}$$

Assume that the flow is developed. No slip at the nozzle plate (z=0) and no stress at the top of the ink layer (z=h) gives the following boundary conditions:

$$u(0) = v(0) = 0 \tag{4.10}$$

$$\left.\frac{\partial u}{\partial z}\right|_{z=h} = \left.\frac{\partial v}{\partial z}\right|_{z=h} = 0 \tag{4.11}$$

Solving the momentum equations (4.7) and (4.8) using the boundary conditions (4.10) and (4.11) results in the following velocity profiles:

$$u(z) = \frac{1}{2\mu}\frac{\partial p}{\partial x} z(z - 2h) \tag{4.12}$$

$$v(z) = \frac{1}{2\mu}\frac{\partial p}{\partial y} z(z - 2h) \tag{4.13}$$

The average velocity in the x-direction is given by

$$\bar{u} = \frac{1}{2\mu}\frac{1}{h}\frac{\partial p}{\partial x}\int_0^h z(z-2h)dz = -\frac{h^2}{3\mu}\frac{\partial p}{\partial x}. \tag{4.14}$$

In a similar way for the y-direction,

$$\bar{v} = \frac{1}{2\mu}\frac{1}{h}\frac{\partial p}{\partial y}\int_0^h z(z-2h)dz = -\frac{h^2}{3\mu}\frac{\partial p}{\partial y}. \tag{4.15}$$

This can be written as:

$$\bar{\vec{v}} = -\frac{h^2}{3\mu}\nabla_H p \tag{4.16}$$

Substitution of equation (4.16) in equation (4.9) gives:

$$\frac{\partial h}{\partial t} + \nabla_H \cdot (h\bar{\vec{v}}) = \frac{\partial h}{\partial t} + \nabla_H^2\left(-\frac{h^3}{3\mu}p\right) = 0 \tag{4.17}$$

This derivation is analogous to the derivation of the Hele-Shaw flow [SCH60].

4.3 Potential flow theory

For a creeping flow with a constant, time independent layer thickness equation (4.17) can be written as

$$\nabla_H^2\left(-\frac{h^3}{3\mu}p\right) = \nabla_H^2\Phi = 0. \tag{4.18}$$

The average velocity can be described as the gradient of a potential Φ, where the potential Φ satisfies the Laplace equation (4.18). This makes it possible to describe the flow on the nozzle plate with potential flow theory.

Because the layer thickness is small compared to the horizontal scales of the flow the flow is assumed to be two-dimensional. For a two dimensional incompressible irrotational flow in polar co-ordinates $\vec{v} = (v_r, v_\theta)$, the continuity equation is:

$$\frac{1}{r}\frac{\partial}{\partial r}(rv_r) + \frac{1}{r}\frac{\partial}{\partial \theta}(v_\theta) = 0. \tag{4.19}$$

The flow can be described by the scalar stream function, Ψ, which is defined as:

$$v_r = \frac{1}{r}\frac{\partial \Psi}{\partial \theta},\quad v_\theta = -\frac{\partial \Psi}{\partial r} \tag{4.20}$$

To get a better physical understanding of the stream function consider a streamline in the (r,θ)-plane as shown in figure 4.2.

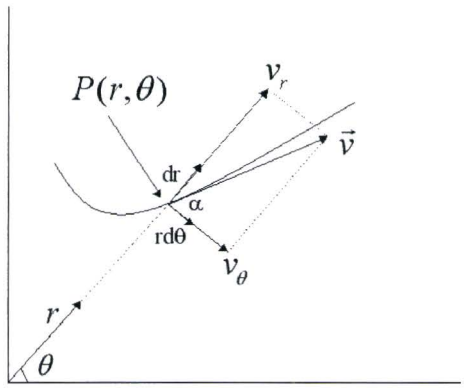

Figure 4.2. Streamline in the (r,θ)-plane.

For every point P on the streamline, the direction of the speed $\vec{v}$ is along the tangent to the streamline. Due to geometric reasons,

$$\tan\alpha = \frac{dr}{rd\theta} = \frac{v_r}{v_\theta} \rightarrow v_\theta dr = rv_r d\theta, \tag{4.21}$$

for all points on the streamline. The total differential of $\Psi(r,\theta)$ for a displacement along the streamline is given by:

$$d\Psi = \frac{\partial\Psi}{\partial r}dr + \frac{\partial\Psi}{\partial\theta}d\theta = -v_\theta dr + rv_r d\theta = 0. \tag{4.22}$$

This results in dΨ=0 along a streamline; streamlines are lines of constant Ψ.

An irrotational 2D flow can be described by the velocity potential, Φ, defined as:

$$v_r = \frac{\partial\Phi}{\partial r},\ v_\theta = \frac{1}{r}\frac{\partial\Phi}{\partial\theta}. \tag{4.23}$$

Lines with $d\Phi$=0 are called equipotential lines.

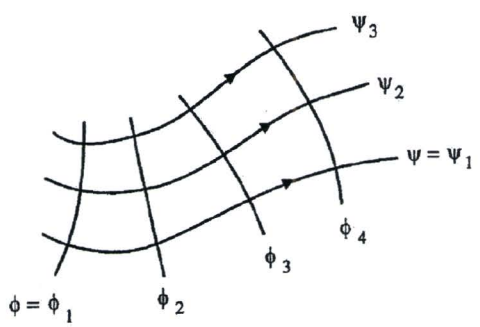

Figure 4.3: Streamlines and equipotential lines

Together the streamlines and the equipotential lines form an orthogonal system (figure 4.3):

$$\nabla\Phi \cdot \nabla\Psi = \frac{\partial\Phi}{\partial r}\frac{\partial\Psi}{\partial r} + \frac{1}{r^2}\frac{\partial\Phi}{\partial\theta}\frac{\partial\Psi}{\partial\theta} = -v_r v_\theta + v_\theta v_r = 0. \tag{4.24}$$

In order to classify the experimental results, that will be discussed in chapter 6, some examples of potential flows are presented in the next sections.

4.3.1 Uniform parallel flow

For a parallel flow with a velocity V with an angle α with respect to the x-axis the stream function is defined as:

$$\Psi(x, y) = rV(\cos\alpha\sin\theta - \sin\alpha\cos\theta) \tag{4.25}$$

and the velocity potential is defined as

$$\Phi(x, y) = rV(\cos\alpha\cos\theta + \sin\alpha\sin\theta), \tag{4.26}$$

both are expressed in cylindrical co-ordinates.

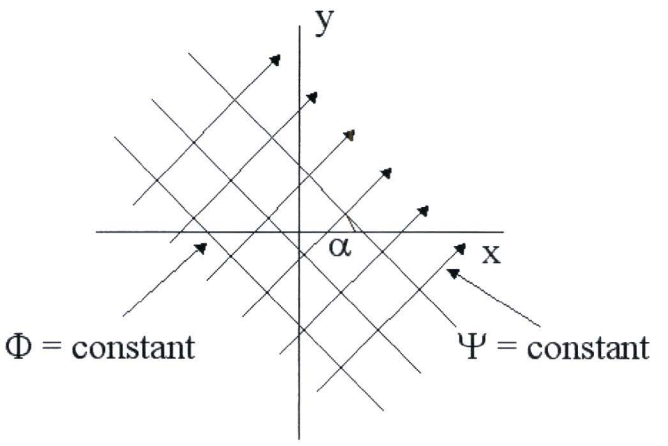

Figure 4.4: equipotential lines (Φ = constant) and streamlines (Ψ = constant) of a uniform flow

The velocity components can be calculated from the stream function (4.25) and the velocity potential (4.26):

$$v_r = \frac{\partial\Phi}{\partial r} = \frac{1}{r}\frac{\partial\Psi}{\partial\theta} = V(\cos\alpha\cos\theta + \sin\alpha\sin\theta) \tag{4.27}$$

$$v_\theta = \frac{1}{r}\frac{\partial\Phi}{\partial\theta} = -\frac{\partial\Psi}{\partial r} = V(-\cos\alpha\sin\theta + \sin\alpha\cos\theta) \tag{4.28}$$

4.3.2 Source/sink flow

For a source of strength N (m^2/s) the stream function is defined as

$$\Psi(\theta) = \frac{N}{2\pi}\theta, \tag{4.29}$$

and the velocity potential is defined as

$$\Phi(r) = \frac{N}{2\pi}\ln r, \tag{4.30}$$

both are expressed in cylindrical co-ordinates.

The velocity components can be calculated from the stream function (4.29) and the velocity potential (4.30):

$$v_r = \frac{\partial\Phi}{\partial r} = \frac{1}{r}\frac{\partial\Psi}{\partial\theta} = \frac{1}{2\pi}\frac{N}{r} \tag{4. 31}$$

$$v_\theta = \frac{1}{r}\frac{\partial\Phi}{\partial\theta} = -\frac{\partial\Psi}{\partial r} = 0 \tag{4.32}$$

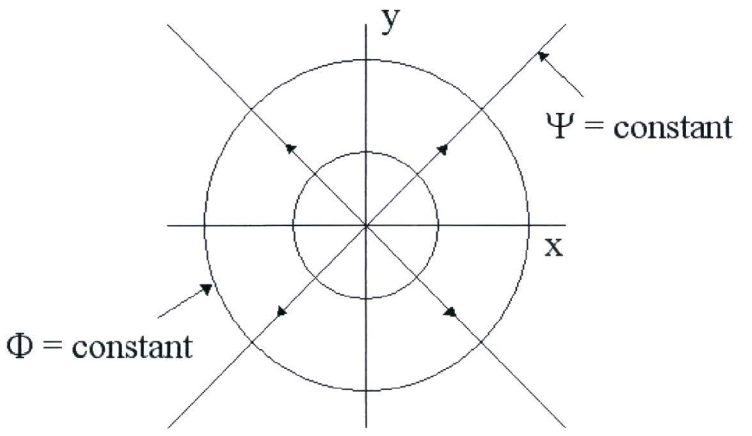

Figure 4.5: equipotential lines (Φ = constant) and streamlines (Ψ = constant) of a point source in the origin.

The velocity magnitude is given by

$$|v| = \sqrt{v_r^2 + v_\theta^2} = \frac{1}{2\pi}\frac{N}{r} \tag{4.33}$$

The velocity field due to a sink equals the velocity field due to a source by replacing N = –N as the strength of the sink.

4.3.3 Dipole flow

Imagine the combination of a source of strength Q in (-Δx,0) and a sink of strength –Q in (Δx,0). In the limit Q↑∞, Δx→0, QΔx=K=constant, the resulting field is a dipole field.

For a dipole of strength K (m^3/s) the stream function is defined as

$$\Psi(r,\theta) = \frac{-K\sin\theta}{r}. \tag{4.34}$$

The potential velocity is defined as,

$$\Phi(r,\theta) = \frac{K\cos\theta}{r}, \tag{4.35}$$

both expressed in cylindrical co-ordinates.

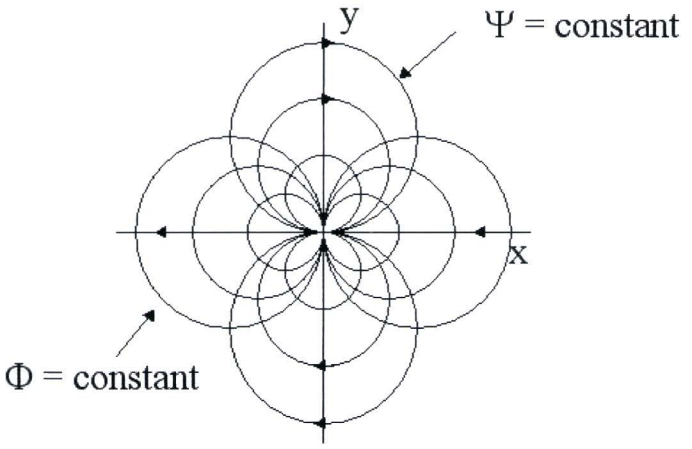

Figure 4.6: equipotential lines (Φ = constant) and streamlines (Ψ = constant) of a dipole in the origin.

The velocity components can be calculated from the stream function (4.34) and the potential velocity (4.35):

$$v_r = \frac{\partial\Phi}{\partial r} = \frac{1}{r}\frac{\partial\Psi}{\partial\theta} = -\frac{K\cos\theta}{r^2} \tag{4.36}$$

$$v_\theta = \frac{1}{r}\frac{\partial\Phi}{\partial\theta} = -\frac{\partial\Psi}{\partial r} = -\frac{K\sin\theta}{r^2} \tag{3.37}$$

The velocity magnitude is given by

$$|v| = \sqrt{v_r^2 + v_\theta^2} = \frac{K}{r^2}\sqrt{\cos^2\theta + \sin^2\theta} = \frac{K}{r^2} \tag{4.38}$$

4.3.4 Non uniform layer thickness

In the previous sections it is assumed that the layer thickness is constant and time independent. A non-uniform layer thickness will cause a deviation from the previous descriptions of potential flows. This is a result of the continuity equation.
Assume the layer thickness, h, is only dependent on r. For a sink of strength N, the velocity magnitude is given by:

$$|v| \propto 1/rh(r) \tag{4.39}$$

Assume, for example, that $h(r) \propto r$, this results in a r^{-2} dependence of the velocity magnitude. Generally, the ink layer thickness neither is cylinder symmetrical nor only dependent on the distance from the nozzle.
To get a better picture of the deviations from the potential flows, caused by non uniform layer thickness, the properties (assuming $|v| \propto 1/rh(x,y)$) of a sink surrounded by an ink layer with a linear x-dependence in the layer thickness are shown in figure 4.7.

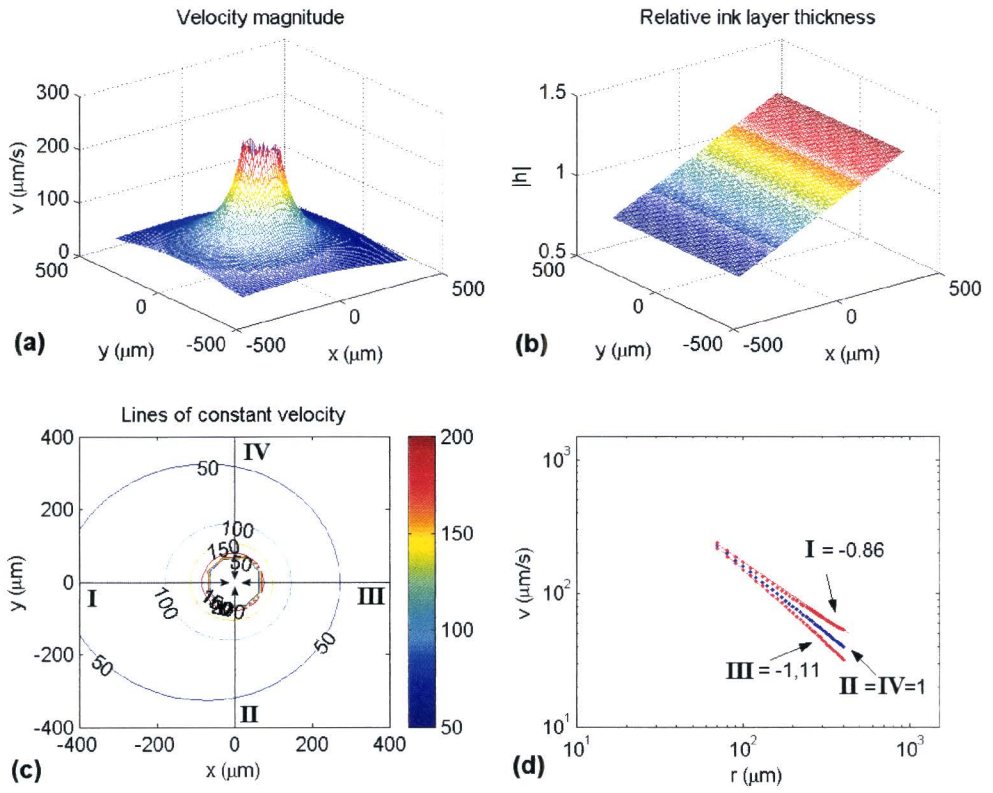

Figure 4.7: (a) Velocity magnitude of the flow near a sink in (x,y)=(0,0) influenced by the non uniform layer thickness. (b) Relative thickness of the ink layer, a first order polynomial in x. (c) Lines of constant velocity. (d) Velocity magnitude as a function of the distance from the nozzle plotted in double logarithmic scaling to show the deviation in r-dependence from a sink surrounded by a ink layer of uniform thickness.

In figure 4.7d the velocity magnitude as function of the distance from the nozzle is plotted when approaching the sink from the low x-direction (I) from the high x-direction (III) and from the low y-direction (II) and high y direction (IV). The plot clearly shows the spreading in the r-dependence due to the non-uniform layer thickness.

4.4 Forces acting on the ink layer

As discussed in the previous section, the thickness of the ink layer is generally not uniform, which causes deviations from the description by potential flow.
Two important forces acting on the ink layer are surface tension and gravity. Gravity causes the ink layer to form droplets (figure 4.8a), while surface tension causes the ink layer to spread (figure 4.8b).

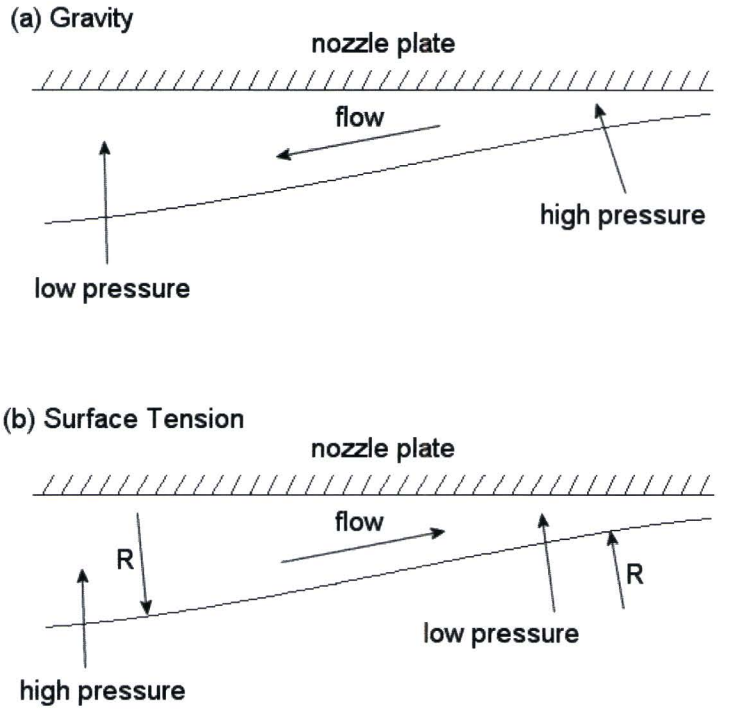

Figure 4.8: The ink layer is situated at the bottom of the printhead. (a) Due to gravity, the pressure in the ink layer is relatively high when the ink layer is thin, and relatively low when the ink layer is thick. This causes a pressure gradient that causes a flow of ink toward the thickest part of the ink layer. (b) The curvature (R) of the ink layer surface causes a pressure gradient, which tends to spread the ink layer.

Assume a source of ink in the ink layer on the nozzle plate; for example ink leaking. This will locally cause a relatively large ink layer thickness. Depending on the absolute thickness of the ink layer, gravity will cause the formation of a droplet, while the surface tension will spread the ink. In the case of a small disturbances and thin ink layer, surface tension will cause a flow of ink from the nozzle.
Generally speaking, for thin ink layers, surface tension acts as a driving force and can cause stationary flows on the nozzle plate.

4.4.1 Spreading of the ink layer on the nozzle plate

As already discussed in chapter 4.2, for a creeping flow the Navier Stokes equations reduce to $grad(p) = \mu \nabla^2 \vec{v}$. The radial component of this equation is:

$$\frac{\partial p}{\partial r} = \mu \frac{\partial^2 u_r}{\partial z^2} \tag{4.40}$$

This equation can be solved for u_r by imposing the boundary conditions no slip at the nozzle plate and no stress at the ink surface. Averaging the velocity results in:

$$\bar{u}_r(z) = -\frac{h^2}{3\mu}\frac{\partial p}{\partial r}. \tag{4.41}$$

Since the influence of a velocity component u_z is neglected, the continuity of mass can be written as:

$$\frac{\partial h}{\partial t} + \frac{1}{r}\frac{\partial}{\partial r}\left(rh\bar{u}_r\right) = 0 \tag{4.42}$$

The pressure in equation (4.41) is determined from a balance of hydrostatic pressure and the pressure that arises from the surface curvature and is given by the Young-Laplace equation:

$$p = \sigma\left(\frac{1}{R_1} + \frac{1}{R_2}\right) - \rho g h. \tag{4.43}$$

R_1 and R_2 are the main surface curvature radii of the ink layer, h is the ink layer thickness and σ is the surface tension. For distances far from the nozzle (r>>a) the main surface radii are given by:

$$\frac{1}{R_1} \approx -\frac{\partial^2 h}{\partial r^2} \tag{4.44}$$

$$\frac{1}{R_2} \approx -\frac{\sin\alpha}{r} \approx -\frac{1}{r}\frac{\partial h}{\partial r} \quad \text{(for small } \alpha\text{)} \tag{4.45}$$

α is the angle of inclination between the surface of the ink layer and the horizontal. Substitution of equation (4.43) in (4.41) results in:

$$\bar{u}_r(z) = \frac{\sigma}{3\mu}h^2\frac{\partial}{\partial r}\left[\left(\frac{\partial^2 h}{\partial r^2} + \frac{1}{r}\frac{\partial h}{\partial r}\right) + \rho g h\right] \tag{4.46}$$

Substitution of equation (4.46) in equation (4.42) results in:

$$\frac{\partial h}{\partial t} + \frac{1}{r}\frac{\partial}{\partial r}\left(\frac{rh^3}{3\mu}\frac{\partial}{\partial r}\left[\sigma\left(\frac{\partial^2 h}{\partial r^2} + \frac{1}{r}\frac{\partial h}{\partial r}\right) + \rho g h\right]\right) = 0 \tag{4.47}$$

This equation is very similar to the equation that describes the spreading of a viscous drop under influence of gravity and surface tension. No analytic solution to this non-linear partial differential equation is available.
An additional problem arises near the contact line of the ink layer. The boundary condition of no slip at the nozzle plate can not hold along the contact line, since the boundary between the ink layer and the nozzle plate is obviously in motion.

By assuming a thin, submicron scale "precursor film", in which intermolecular forces become relevant (mainly van der Waals) it is possible to solve the problem of a spreading droplet. This requires meso-scale modelling of the wetting of the nozzle plate [MID95].

4.5 Acoustic streaming

4.5.1 Mechanism

As an acoustic wave travels through a medium it may be absorbed. The momentum loss of the acoustic field manifests itself as a flow of the liquid. This second order, steady, circulatory fluid motion produced by acoustic fields in viscous flows is called acoustic streaming.

A qualitative idea of the generation of acoustic streaming can be obtained by considering acoustic radiation pressure acting on a fluid element in which acoustic waves propagate. Since the acoustic energy attenuates due to viscosity along the propagation path through a fluid element there is a difference in pressure between the input and the output of the fluid element. This pressure difference will drive the fluid element in the direction of the sound propagation.

Absorption due to viscosity of the medium is essential in the generation of acoustic streaming. Generally speaking, viscosity suppresses fluid motion, but it acts as a source of the driving force in the generation of acoustic streaming.
It is also important to note that acoustic streaming is not only produced by continuous waves but also by burst waves. [MIT98]

A second type of streaming occurs near small obstacles. Instead of frictional forces it arises between a boundary and a medium carrying vibrations. This time-independent circulation only occurs in a small region of the fluid. Because of the restricted scale of the circulation it is commonly termed microstreaming. Microstreaming can specifically occur as a result of the oscillations of an acoustic driven bubble in a sound field [LEI94].

4.5.2 Streaming on the nozzle plate

The jetting of droplets, or more general the vibration of the meniscus in the nozzle can give rise to capillary surface waves in the ink layer. These capillary waves can cause ink flow. More generally, oscillatory fluid motion can give rise to microstreaming.

Figure 4.8 shows the streamlines of the flow induced by an oscillating bubble near a wall. The oscillations refer both to translation and volume changes.

The oscillating bubble in figure 4.8 induces a three dimensional form (cylinder symmetry) of microstreaming. Since the vertical dimensions of the ink layer on the nozzle plate are very small compared to the horizontal dimensions it is quite unlikely that a flow field like figure 4.8 will occur in the ink layer on the nozzle plate.

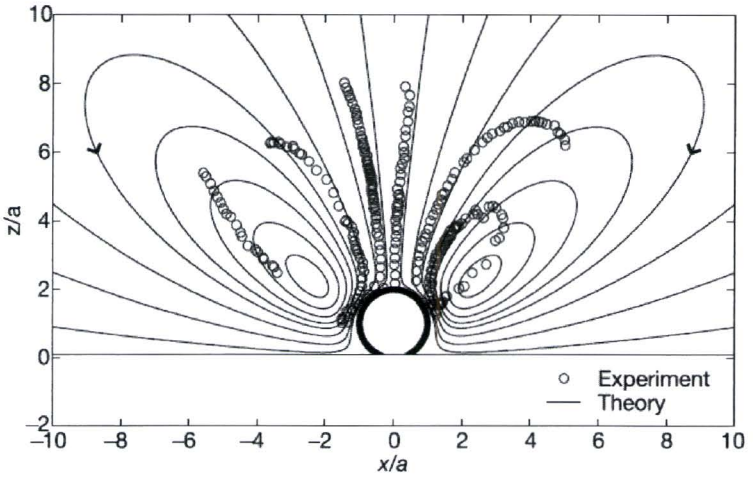

Figure 4.8: Streamlines of the flow near an oscillation bubble near a wall superimposed on a number of measured trajectories. [HIL03]

In the case of the thin ink layer on the nozzle plate it is more likely that a quasi 2D-flow field will occur in the plane of the nozzle plate.
An equivalent quasi 2D-flow is presented in figure 4.9. A cylinder is stimulated by a standing wave of 512 Hz. This causes displacements in the plane of the photograph.

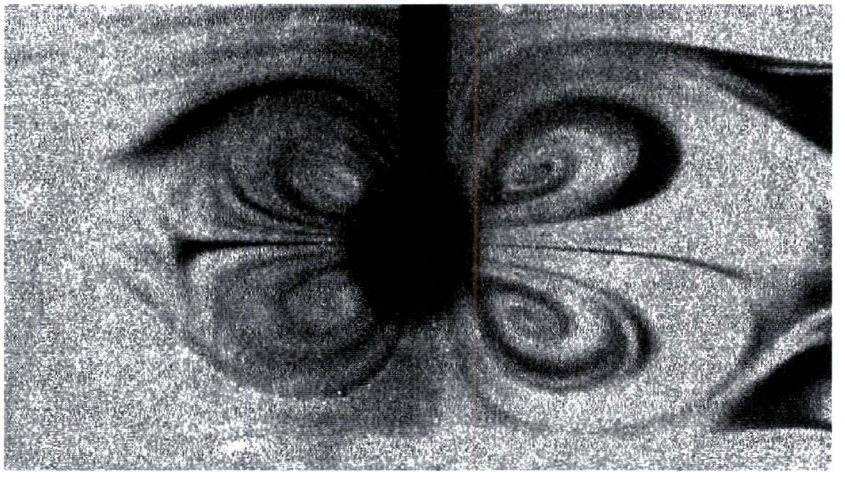

Figure 4.9: flow pattern in air surrounding a cylinder of diameter 2-4 mm, stimulated with a standing wave with a frequency of 512 Hz. The displacements due to the sound wave are in the plane of the photograph. The axis of the cylinder is normal to the plane and coincides with the displacement antinode. [AND32]

If the nozzle causes microstreaming on the nozzle plate it is likely that the flow field in the ink layer on the nozzle plate resembles the flow pattern presented in figure 4.9.
If microstreaming occurs at the nozzle plate it will appear as a steady circulatory quadrupole like flow.

5. Experimental methods

5.1 Experimental setup

A default setup, used to do research on the functioning of printheads, was available at Océ. This setup can be divided into two parts: the optical part and the part for driving the head. An extensive description of the apparatus used is presented in appendix A.

The part to drive the head is controlled by a PC, which is used to program the wavegenerator and to control the switchboard. A schematic view of the setup is shown in Figure 5.1.

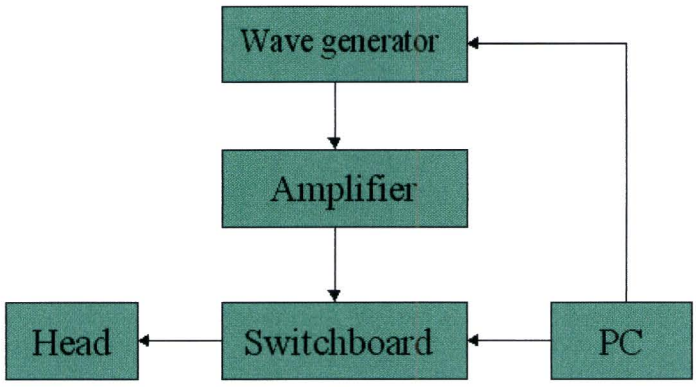

Figure 5.1: schematic view of the setup used to drive the head

The waveform generator, a Philips PM5150, generates the actuation pulse for the piezo. In general this pulse has a trapezium shape with a certain amplitude and frequency. This frequency will be referred to as the DOD frequency, f_{DOD}. All details of the pulse can be programmed using the PC.
The signal from the waveform generator is amplified and sent to the switchboard. The switchboard is used to control which ink channel is actuated and is controlled by the PC.
Using this setup it is possible to control every ink channel independently and it is possible to send an arbitrary waveform to any piezo, therefore controlling each ink channel individually.

In the standard optical setup the jetted droplets were visualised stroboscopically. This makes it possible to use a standard 25-fps CCD-camera to observe the jetted droplets. From these recordings, droplet properties as speed, size and angle can be obtained.
To observe the nozzle plate instead of the jetted droplets, the optical setup is adapted by mounting a mirror at a 45-degree inclination just below the nozzle plate as shown in figure 5.2.

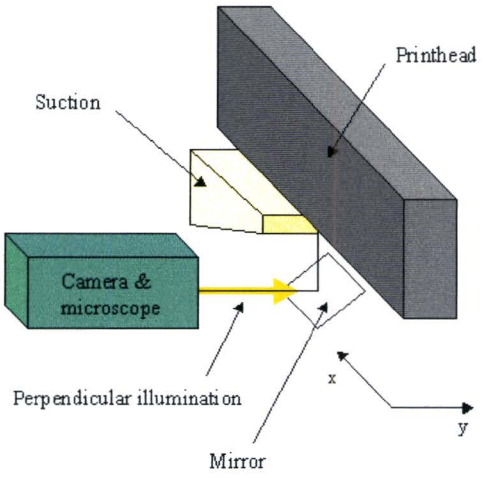

Figure 5.2: optical part of the setup.

An airflow is generated by applying suction between the nozzle plate and the mirror. This airflow prevents the jetted droplets from reaching the mirror.
The nozzle plate is observed using a 25-fps Sony CCD camera connected to an Olympus microscope.
The nozzle plate is visualised via the microscope, which results in a perpendicular illumination. Using two linear actuators (x and y direction) it is possible to move the nozzle plate with respect to the mirror. This makes it possible to observe the entire surface of the nozzle plate at various magnifications.

5.2 Nozzle plate visualisation

The setup described in chapter 5.1 makes it possible to observe the entire nozzle plate surface. For further examination it is necessary to acquire these images in a digital form. Therefore two Labview programs are developed.

The first program uses the framegrabber in the PC and the two linear actuators on the printhead to take snapshots of the nozzle plate along a predetermined path in the x-y space. These separate images are composed into one high-resolution image of the entire nozzle plate. This makes it possible to map the wetting of the entire nozzle plate. The time needed to entirely map the nozzle plate depends on the desired resolution, but a 2 pix/µm resolution (56 Mpixel) is completed in less than 2 minutes.

An image obtained using the described program is shown in figure 5.3. This figure shows the ink layer on the nozzle plate of a printhead shortly after a pressure step of 5 mBar (with respect to the ambient) is applied to the ink head.

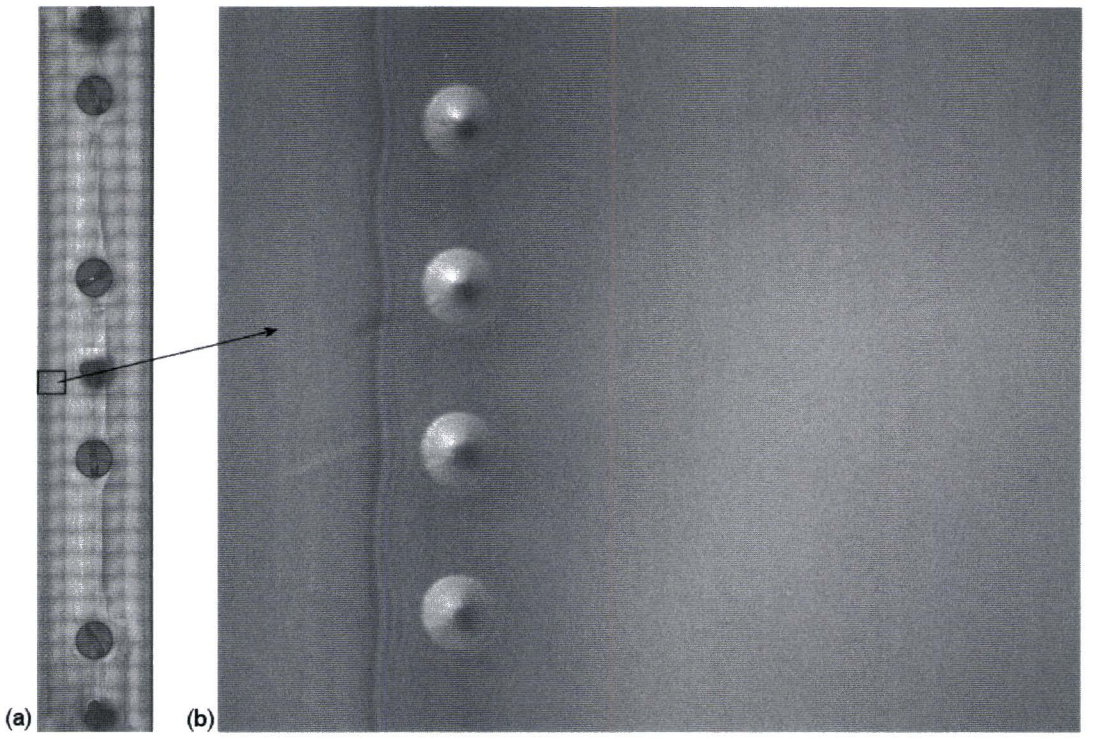

Figure 5.3: (a) the composite image of 128 separate snapshots. (b) one snapshot, showing from left to right: the dry nozzle plate surface, the liquid front, the nozzles and the wet nozzle plate surface.

A second program was developed to take a sequence of snapshots within a specific time period at the same position at the nozzle plate to monitor the movement of the ink layer. Experiments with the framegrabber have shown a maximum framerate of 2-fps.

A timelapse measurement of the ink layer on the nozzle plate, after a 0,5 second 5 mBar pulse is applied, is presented in figure 5.4.

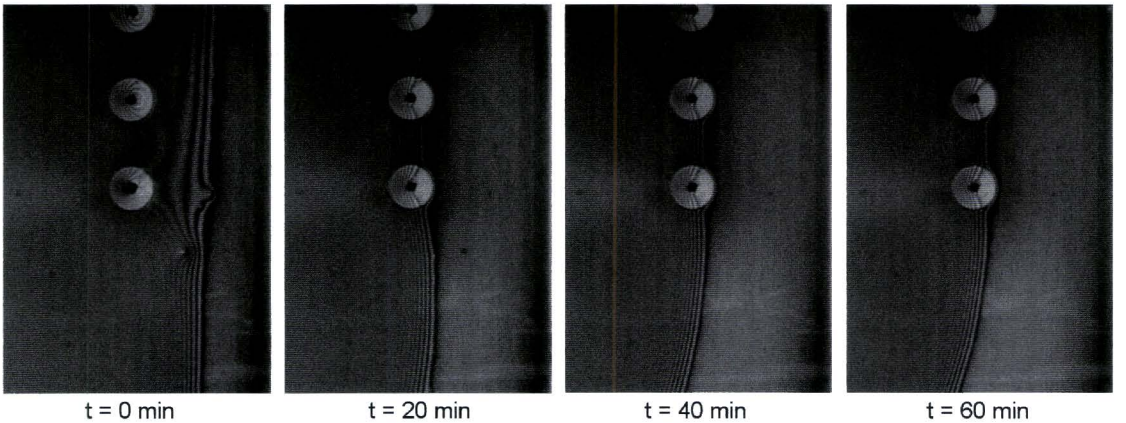

Figure 5.4: Timelapse images of the ink layer on the nozzle plate.

From figure 5.4 it can be concluded that the movement of the contact line of the ink layer is very slow. The contact line is pinned between the nozzles.

When the head is tilted over a small angle with respect to the vertical, it is clear that on the time scales as depicted in figure 5.4 the gravity has small influence on the movement of the ink layer.
Because the ink has no structure and is transparent it is not possible to obtain information on the movement of the ink layer at greater distances from the contact line.

5.3 PTV Experiments

During the construction of the optical setup it was often noticed that there was light scattering visible, from moving particles, when being illuminated under a small angle ($\theta<30°$) with respect to the nozzle plate surface. These particles were probably present in the ink, but it is also possible that it was dust from the surroundings.
Assuming the small particles to follow the ink flow, the flow field in the ink layer can be determined by measuring the speed of the particles.
Figure 5.5 shows a snapshot of the nozzle plate surrounding a nozzle, illuminated under a small angle with respect tot the nozzle plate. This snapshot is taken at magnification 8 using a 2 x objective of the Olympus microscope. Because the very small amount of scattered light, the Sony camera is substituted by a high sensitivity Watec camera (a comparison is given in Appendix B).

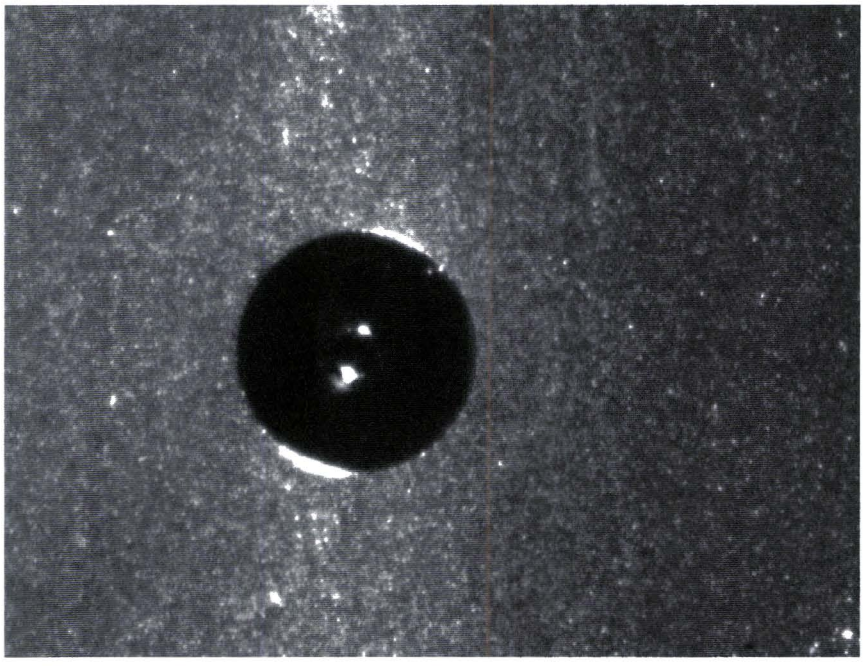

Figure 5.5: snapshot of the nozzle plate using a small angle illumination, showing the saucer within the center the nozzle.

Using this illumination method, not only the scattering of light on the dust particles is visible, but also the scattering of light on the nozzle plate structure. To distinguish the light scattered by particles from the light scattered by the structure of the nozzle plate, a background correction is performed by taking the difference of two subsequent frames.

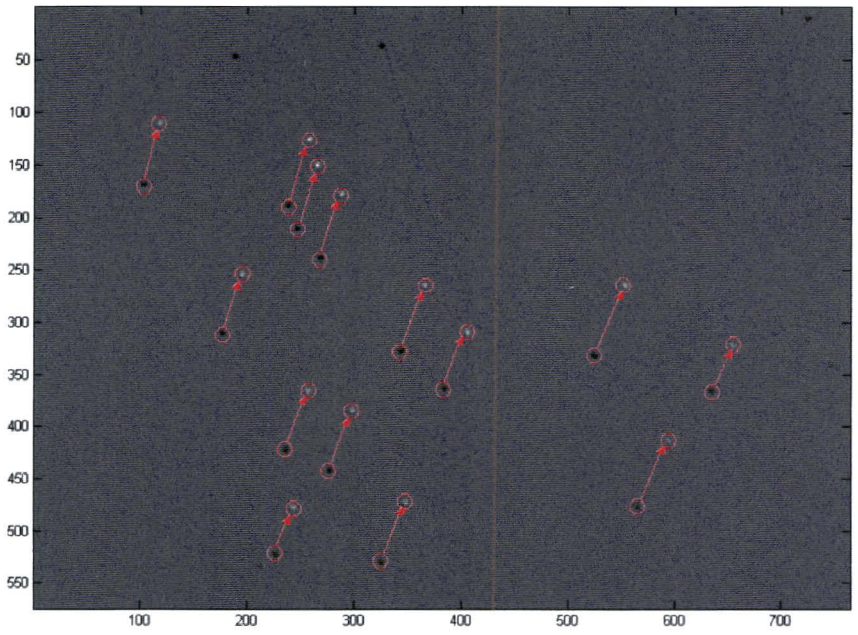

Figure 5.6: difference of two subsequent frames. A circle indicates the particles in frame n and n+1. The arrows indicate the motion from frame n to n+1.

Figure 5.6 shows the difference of two subsequent frames n and n+1. In this image particles are visible at their position in frame n (black particles) and in frame n+1 (white particles). Because the particle positions and the frame rate is known it is possible to calculate the particle speed.

With this in mind, the development of a PTV-script using Matlab was started. The PTV-tracking script consists of the following steps:
1. Background correction by taking the difference between two subsequent frames
2. Locating particles by applying a threshold in pixel intensity
3. Identifying particles by predicting their position.

The flowchart of the PTV-tracking script is shown in figure 5.7

The output of the tracking script is a structure with the position and the frame number of de tracked particles. For postprocessing this data, scripts were developed for drawing the particle lines, calculating the velocity, interpolating the velocity/rotation/divergence field, etc.

5.4 Use of tracer particles

During the first experiments with the PTV toolkit it turned out that the amount of particles is too low for obtaining an accurate velocity field in the ink layer on the nozzle plate. Therefore tracer particles have to be applied, which do not disturb the flow.

The requirements for the tracer particles are:
- Small diameter compared to the thickness of the ink layer
- High temperature stability: stable at temperatures up to 130°C
- Density comparable to the density of the ink: $\rho \approx 1{,}1 \cdot 10^{3}$ kgm^{-3}
- High stability in dispersions

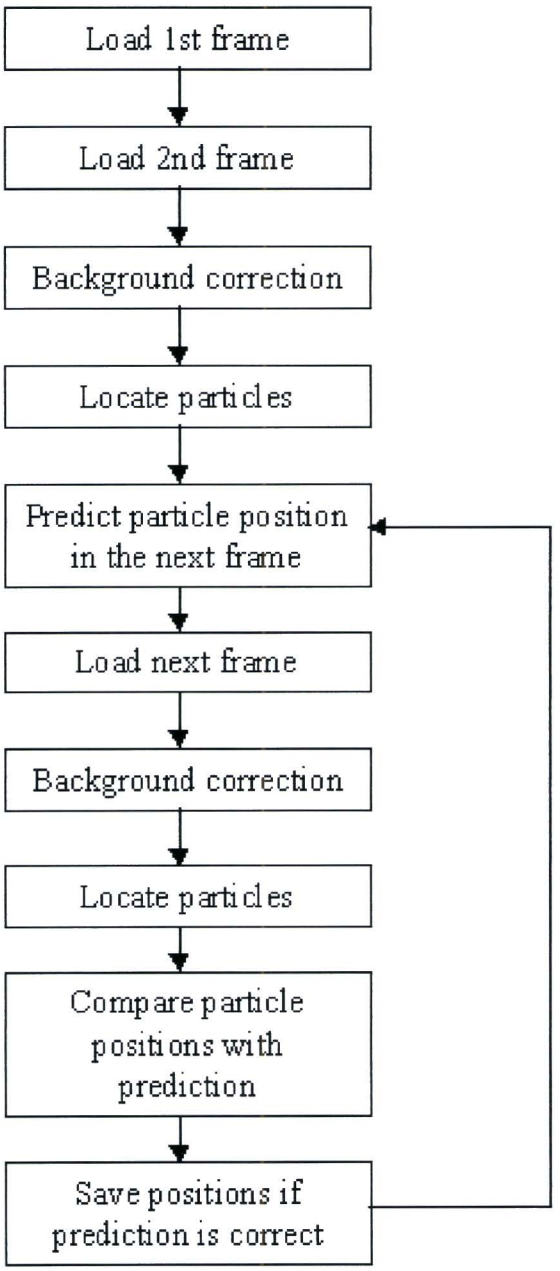

Figure 4.7: flowchart of the PTV-tracking script.

5.4.1 Melamine tracer particles

Experiments with melamine resin particles with a diameter of 2 µm were started. These particles have an excellent monodispersity (0,06 µm standard deviation), a highly uniform spherical shape and offer a high stability in dispersions. The density of the melamine particles is 1,51g/cm^3. The melamine particles were added to 10g ink in a 0,015-weight percentage, which results in $2{,}59 \cdot 10^{13}$ particles/m^3. Assuming an ink layer thickness of 20 µm this results in a particle density of $5{,}18 \cdot 10^8$ particles/m^2.
Although the density of the melamine particles is 50% higher than the density of the ink, no sedimentation was noticed during stirring. To prevent possible sedimentation during solidification of the ink, the ink was poured on a plate of cold aluminium to cool it down very quickly.
Further experiments have shown that melamine particles excellently disperse in ink and do not form any clusters.

5.4.2 Experiments

The particles have been applied on the nozzle plate by melting a piece of solid ink on the nozzle plate. During the experiment it turned out that using perpendicular illumination the particles were perfectly visible.
During the first experiments a deviation in the speed of the ink layer was noticed. An example experiment is shown in figure 5.8. The lines represent the tracked particle lines, which are identified by a unique number.

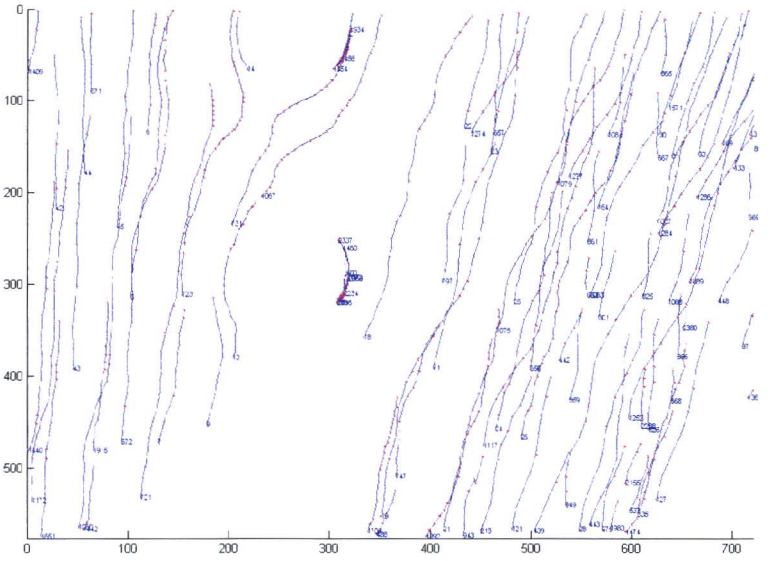

Figure 5.8: particle lines showing an almost parallel flow

Further experiments showed that the deviation in the speed originates from the airflow that is used to bend the ink droplets from the mirror. This is an indication that the airflow is able to influence the behaviour of the ink layer on the nozzle plate.
Removing the suction and substituting it by an injection needle operating at a relatively high pressure (200 mbar) makes the final modification to the experimental setup (figure 5.9).

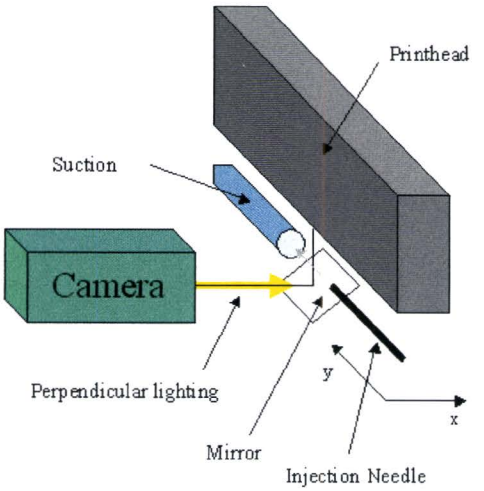

Figure 5.9: final experimental setup

The jetted droplets are blown in a tube with low suction. The needle and the tube are placed just above the mirror. Experiments have shown that the local airflow does not influence the ink layer.

6. Experimental results

In chapter 5 the development of the experimental setup, the software and the measurement method required to perform measurements on the ink layer are described.
In this chapter some first explorative measurements are discussed. In section 6.1 measurements are performed using a jetting actuation pulse. Non-jetting actuation pulses are used to perform measurements on flows caused by an oscillating meniscus. These measurements are discussed in section 6.2.
Finally some remaining research questions are formulated in chapter 6.3.

6.1 Experiments with jetting actuation

Measurements are performed using the Melamine particles. The particles are applied to the nozzle plate surface. After the application of the particles, the jet process is started at 20 kHz using a 553 pulse with an amplitude of 34V. The digital images are acquired using a 25-fps video capture card. This video sequence is analysed using the PTV-toolkit. The resulting particle lines are presented in figure 6.1.

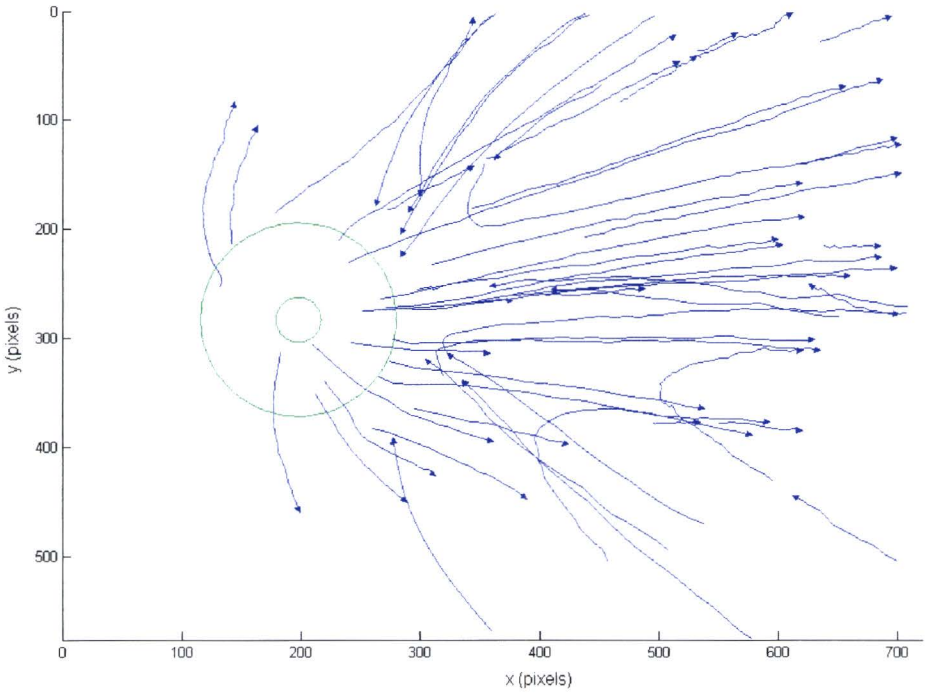

Figure 6.1: The particle lines (in blue) of a nozzle actuated at 20 kHz using a 34 Volt 553 trapezium pulse shown an almost cylinder symmetrical flow at the right side of the nozzle. The nozzle and the saucer are shown in green. Scales are in pixels (1 pixel ≈ 0.75 μm)

Figure 6.1 shows an almost radial flow field at the right side of the nozzle. At the left side no particle lines are visible due to the fact that there was no ink layer present. Above and below the nozzle the other nozzles disturb the flow field. This causes a deviation from the radial character of the flow.

Figure 6.2 shows the two velocity components: v_r, the velocity towards the nozzle, and v_θ, the velocity component perpendicular to v_r.

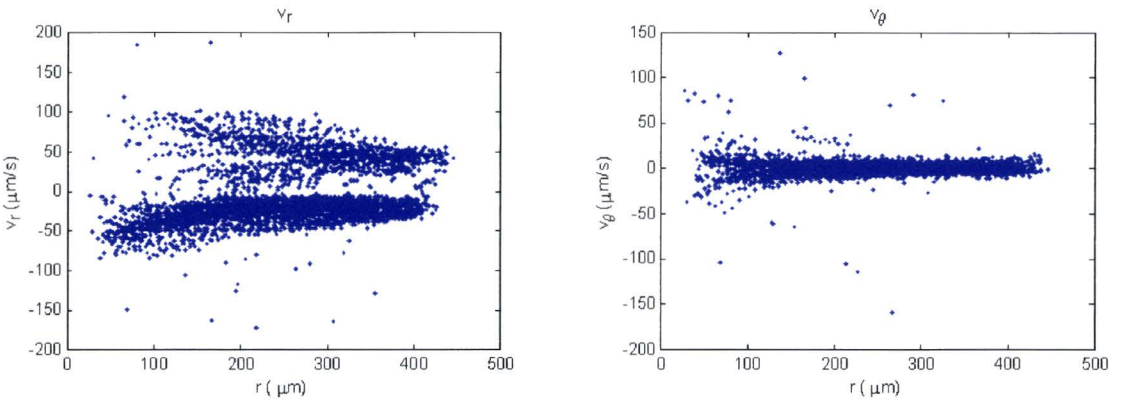

Figure 6.2: Left: velocity towards the nozzle, clearly showing particles moving towards the nozzle and particles moving from the nozzle. Right: velocity in theta direction

From figure 6.2 it can be concluded that the ink flow is almost radial ($v_r >> v_\theta$). It is also apparent that a part of the particles is travelling towards the nozzle, while another part is travelling from the nozzle.

What cannot be seen in figure 6.2, but which is very clear in the video sequence, is that these two different directions of movement occur at the same position and at the same time. In the video sequence it is clearly visible that the ink velocity has two different directions at the same position on the nozzle plate. This can only be explained by the fact that the velocity direction is not uniform in the depth of the picture: at a certain depth the ink is moving towards the nozzle but at another depth the ink is travelling from the nozzle.

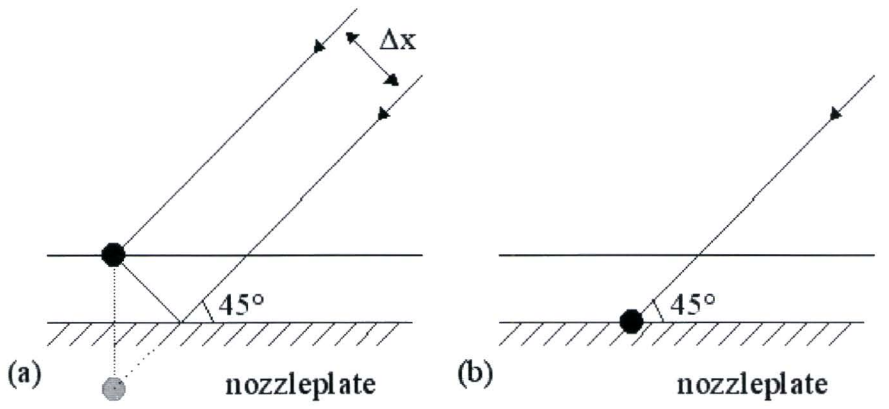

Figure 6.3: Two extremes in vertical particle position (a) Particle at the surface of the ink layer shows a mirror image at an apparent distance Δx. (b) Particle at the surface of the nozzle plate shows no image.

To determine the direction of the ink layer a camera is placed with the optical axis at a 45 degree angle with respect to the nozzle plate. Because the nozzle plate surface

behaves as a mirror, particles in the ink layer will show an image in the mirror. The distance between particle and image particle depends on the z-position of the particle. This offers the possibility to determine z dependent velocity profiles.
From these experiments it can be concluded that the ink at the top of the ink layer moves towards the nozzle and the ink closest to the nozzle plate moves away from the nozzle, which is shown in figure 6.4.

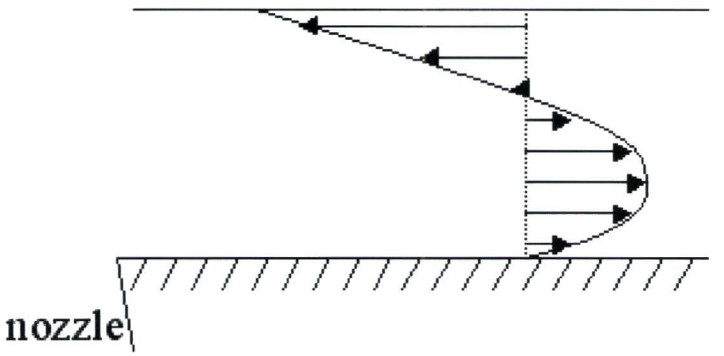

Figure 6.4: velocity profile in the ink layer

Because of the known camera angle, it is possible to calculate the layer thickness from the distance between the real particle and its mirror image. From the measurements it can be concluded that the maximum film thickness is (25±5) µm.

Jetting at different frequencies (5 kHz, 10 kHz, 15 kHz, 20 kHz and 25 kHz) using a 553 pulse with an amplitude of 34V shows that the flow in the ink film depends on the frequency. The results are presented in table 6.1.

Table 6.1: frequency dependent flow in the ink film

Frequency (kHz)	Symmetry	Observed behaviour
5	Cylindrical	Little flow towards the nozzle
10	Cylindrical	Very little flow towards the nozzle
15	Cylindrical	Very strong flow towards the nozzle, resulting in dry surroundings
20	Cylindrical	Two directional flow
25	Cylindrical	Flow towards the nozzle

At 15 kHz a strong flow towards the nozzle occurs. This results in dry surroundings of the nozzle. This process is shown in figure 6.5 at four different points in time. The width of the interference patterns is an indication of the inclination of the ink layer. From this it can be concluded that the surroundings of the nozzle dewet due to the high suction of the nozzle.

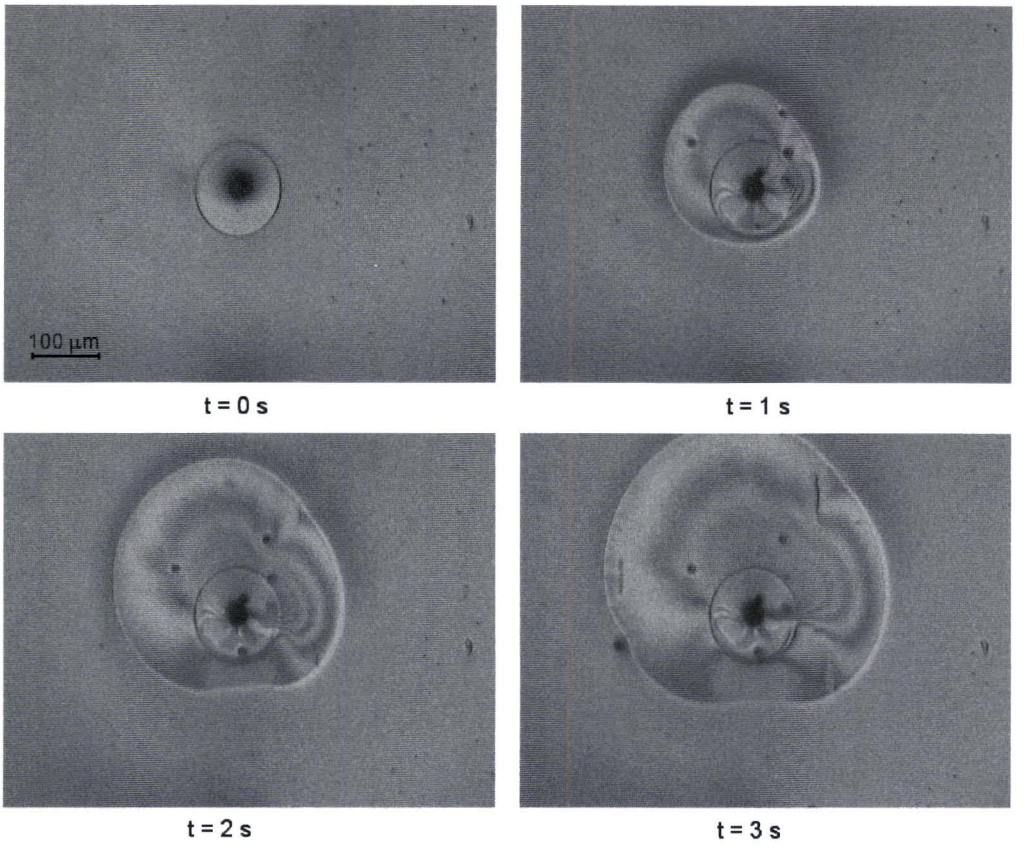

Figure 6.5: Resulting flow when jetting at 15 kHz, 34V, 553 pulse. The image shows the nozzle with the particles in the surroundings at t=0s, t=1s, t=2s and t=3s. Jetting is started at t = 0 s.

Further experiments with a 26 kHz jetting nozzle clearly show the sink like behaviour (figure 6.6)

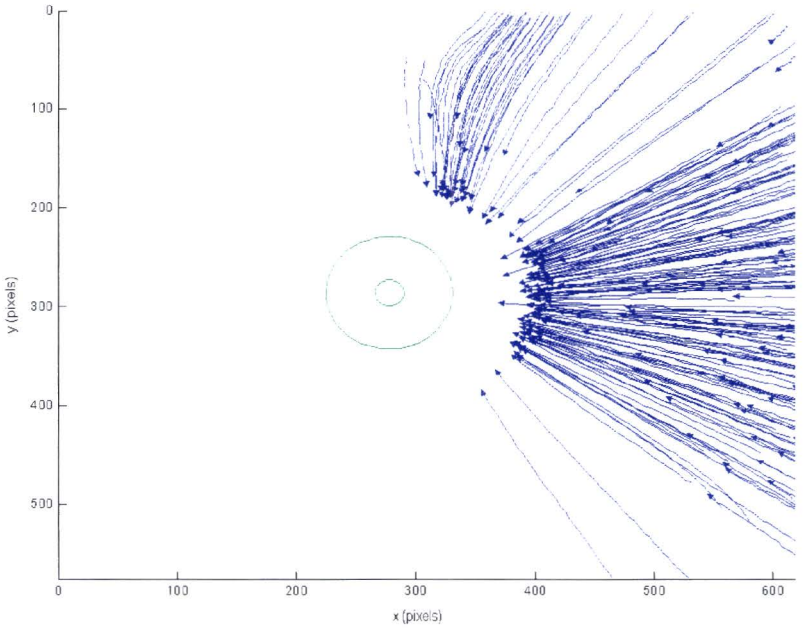

Figure 6.6: The particle lines (in blue) of a nozzle actuated at 26 kHz using the standard pulse show a strong flow towards the nozzle. The nozzle and the saucer are shown in green. Scales are in pixels (1 pixel $\approx$ 1.2 µm).

The particle lines resemble the particle lines of the sink flow field as discussed in paragraph 4.3.
For each detected particle the velocity (and its components) are calculated, which are shown in figure 6.7.

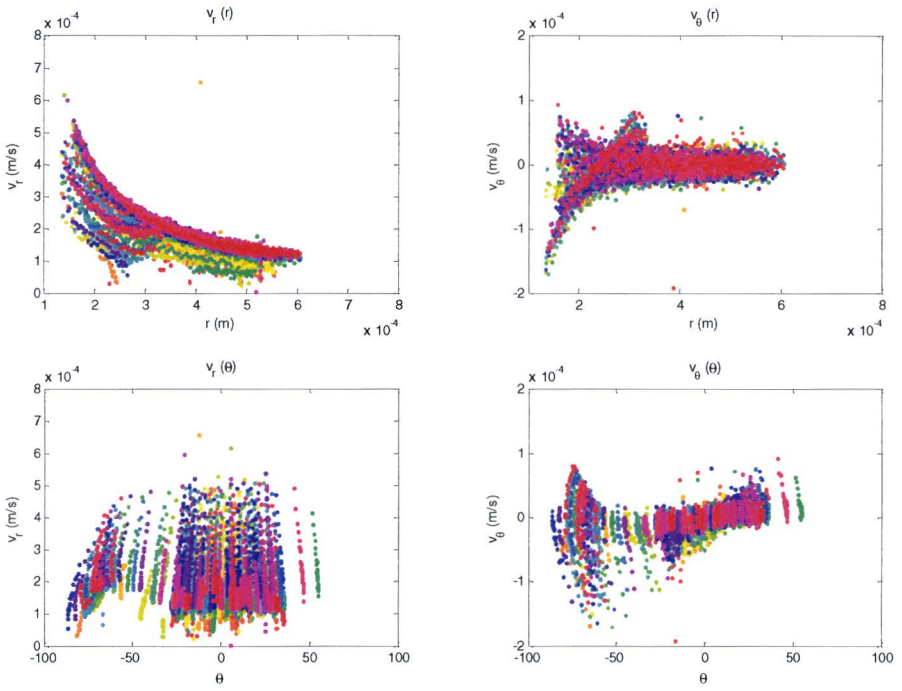

Figure 6.7: starting from the top left in clockwise direction: (a) $v_r(r)$, (b) $v_\theta(r)$, (c) $v_\theta(\theta)$ and (d) $v_r(\theta)$. Each colour represents another particle line.

Since $v_r << v_\theta$ and v_r and v_θ are independent of θ it can be assumed that the flow is almost radial. To further check the resemblance with a sink, the absolute velocity as function of the distance to the nozzle, r is presented in figure 6.8.

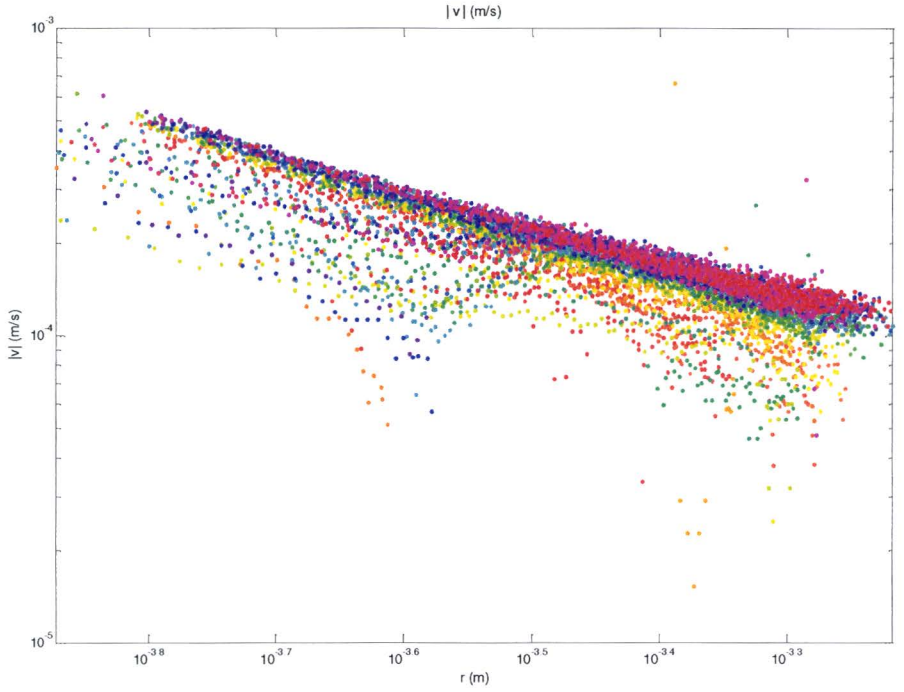

Figure 6.8: Absolute velocity |v|(m/s) as function of the distance to the nozzle r (m) plotted using a double logarithmic scaling.

Assuming a $1/r^n$ dependency of the absolute velocity.

$$v(r) = ar^n \rightarrow \log v(r) = \log(ar^n) = \log a + n \log r \qquad (6.1)$$

Equation (6.1) shows that using a linear fit on double logarithmic scaling, the slope of the fit is equal to n and the intercept is equal to $log\ a$. The results of this fit are presented in figure 6.9.

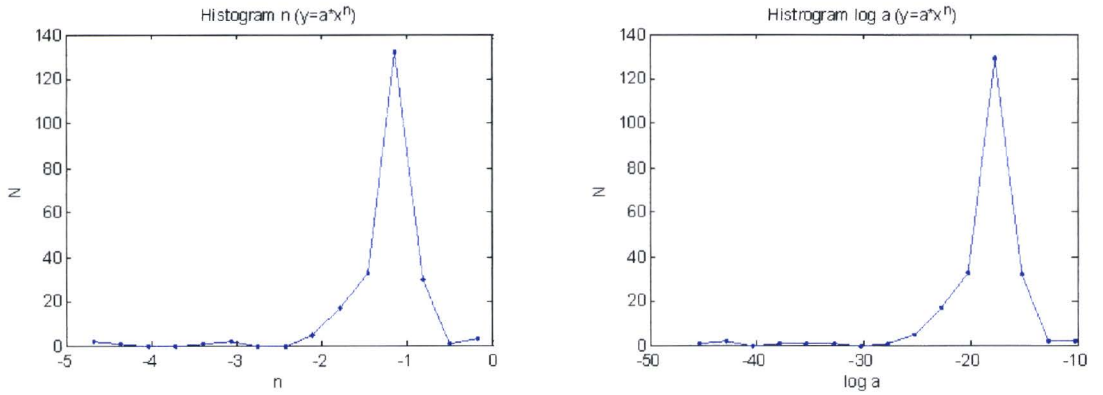

Figure 6.9: (a) histogram of the slopes of the particle lines from figure 5.8. (b) histogram of the axis crossing of the particle lines from figure 5.8.

For a flat 2D sink flow a 1/r dependence is expected: n = -1. Figure 6.9 shows n = (-1,3 ± 0,3) and the sink strength N≈O(e^{-17}) m^2/s.

6.2 Experiments with non-jetting actuation

To further (temporarily) simplify the problem and to check if the oscillations of the meniscus can cause movement in the ink layer, experiments with non-jetting nozzles are performed.
Again Melamine particles are used. After adding these particles, the jet process is started at 20 kHz using a 553 pulse with amplitude of 15V. This amplitude causes oscillations but is not sufficient to form droplets at the nozzle. Figure 6.6 shows the particle lines of the resulting flow in the vicinity of the nozzle.

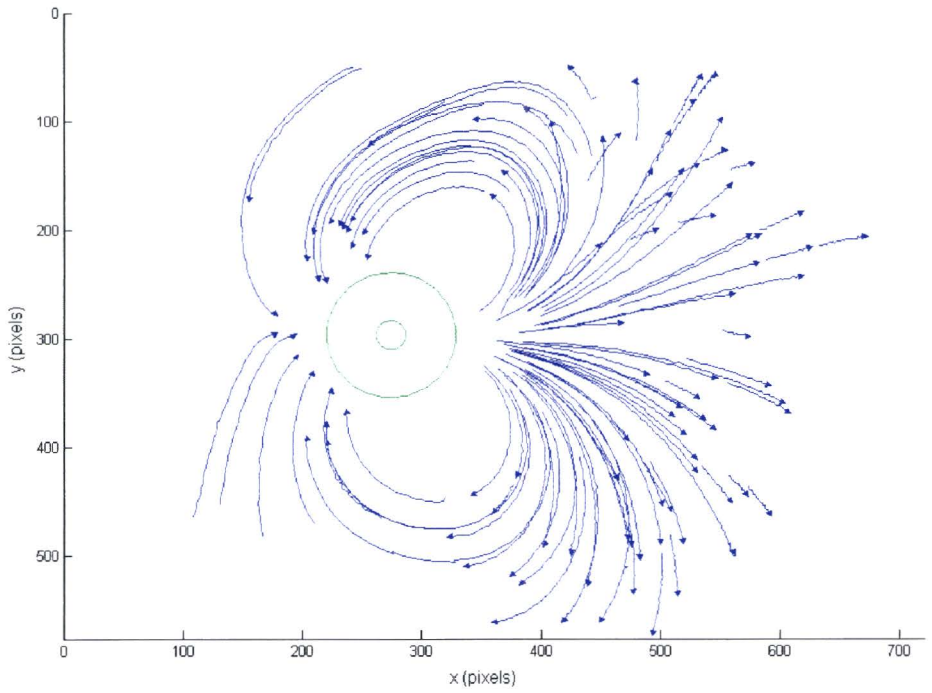

Figure 6.10: The particle lines (in blue) of a nozzle actuated at 20 kHz using a 15 Volt 553 trapezium pulse show a dipole-like flow field. The nozzle and the saucer are shown in green. Scales are in pixels (1 pixel ≈ 1.2 μm).

The particle lines in figure 6.10 clearly resemble the particle lines of a dipole as discussed in chapter 4.3. During the experiments it was striking that the dipole direction was always along the ink layer thickness gradient.

To further investigate the dipole character of the flow, for each detected particle the velocity (and its components) is calculated. These are shown in figure 6.11.

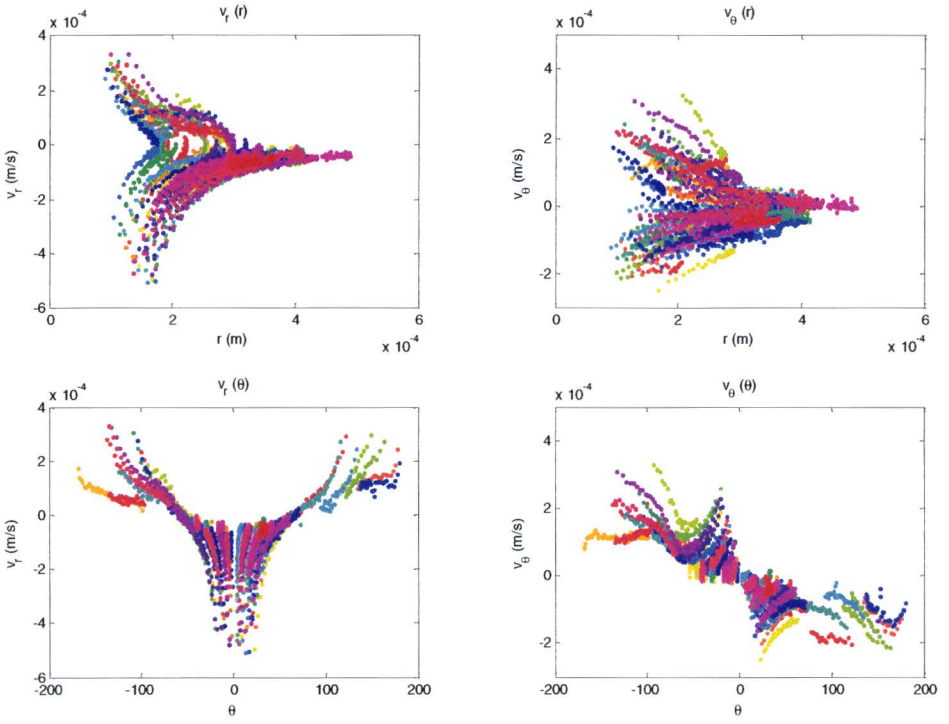

Figure 6.11: starting from the top left in clockwise direction: (a) $v_r(r)$, (b) $v_\theta(r)$, (c) $v_\theta(\theta)$ and (d) $v_r(\theta)$. The different colours represent the different particles.

Figure 6.11 shows that the observed flow is symmetric in $\theta = 0$. The absolute velocity as a function of r is presented in figure 6.12.

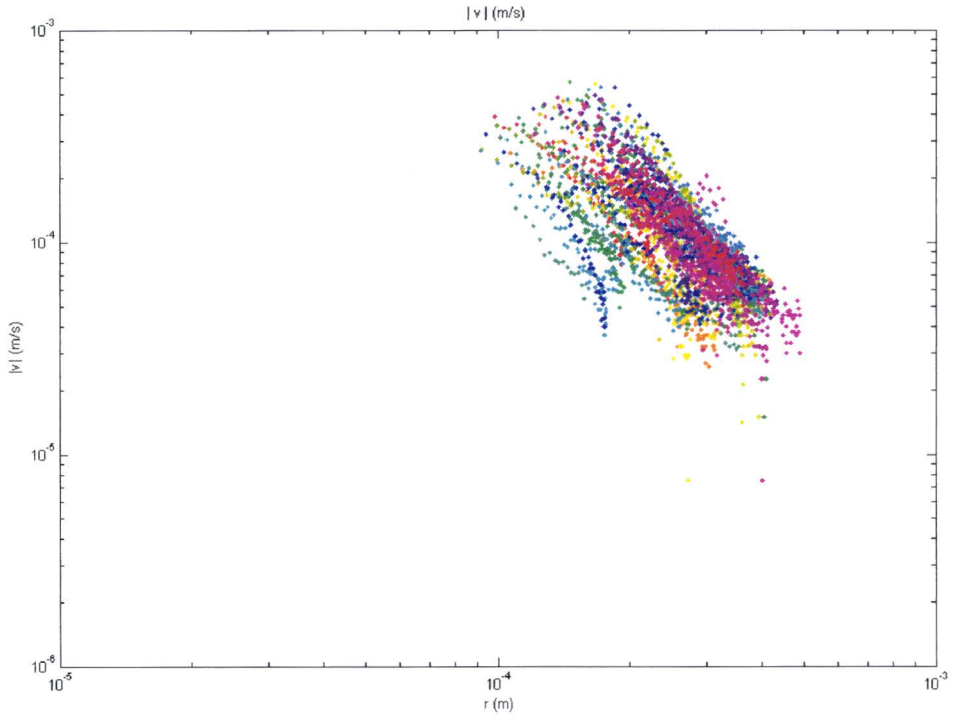

Figure 6.12: Absolute velocity |v|(m/s) as function of the distance to the nozzle r (m) plotted using a double logarithmic scaling.

Again assuming a $1/r^n$ dependency of the absolute velocity, the results for n and a are presented in figure 6.13.

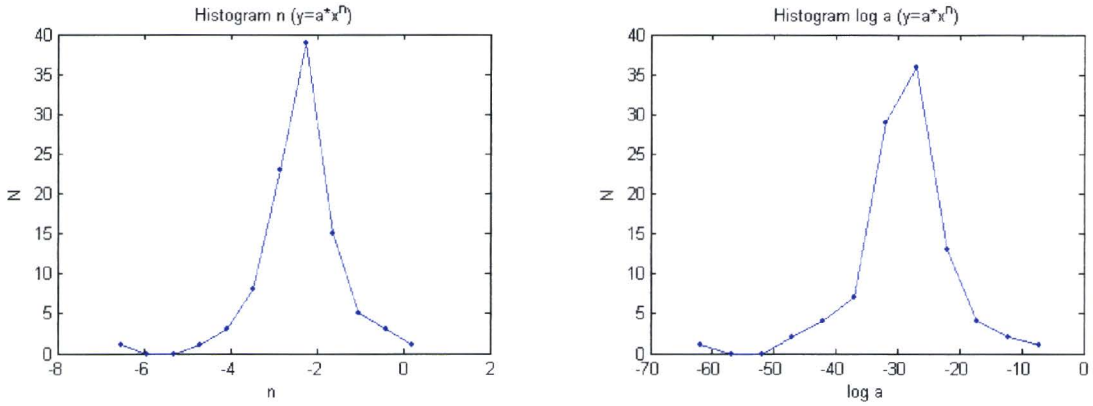

Figure 6.13: (a) histogram of the slopes of the particle lines from figure 4.6. (b) histogram of the axis crossing of the particle lines from figure 4.6.

From equation (4.39) an $1/r^2$ dependency is expected: n = -2. Figure 6.13 shows a measured value of n = (-2,3 ± 0,3). A dipole strength $K \approx O(e^{-30})$ m^3/s is found.

6.3 Discussion

The experiments with jetting pulses show a radial sink like flow in the ink layer. Experiments with non-jetting pulses show a dipole like flow field.

The measurements using jetting pulses show that the behaviour of the flow near the nozzle depends on the DOD frequency but generally shows a sink like behaviour. The small deviation from an exact sink flow field can be caused by a non-uniform ink layer thickness as discussed in chapter 4.3.4.

At 20 kHz there is a strong deviation: a two directional flow occurs. During a frequency sweep with a stepsize of 1 kHz the two directional flow is only observed at 20 kHz. From this it can be concluded that the two directional flow only occurs at a range less than 2 kHz near 20 kHz.

Possible responsible mechanisms are:

1. Overfill or underfill of the nozzle. This depends on the channel acoustics and the nozzle shape.
2. Airflow induced by the jetted droplets. A jetted droplet causes a momentum flux, which subsequently leads to a radial suction of air towards the nozzle. The airflow can exert a force on the top of the ink layer towards the nozzle. This depends on the DOD frequency, droplet size and droplet speed.

Overfill of the nozzle causes a relative large ink layer thickness near the nozzle. Due to this non-uniform ink layer thickness, surface tension causes a pressure gradient (section 4.4), which causes ink to flow from the nozzle. The airflow induced by the jetted droplets exerts a force on the top of the ink layer towards the nozzle. This causes a Couette like velocity profile in the ink layer, as shown in figure 6.4.

The total momentum of the stream of droplets (figure 6.14) increases with frequency. This results in an increasing momentum transfer from the droplets to the air, which will subsequently cause a greater suction of air towards the jet.
Thus the influence of the airflow induced by the jetted droplets increases with increasing frequency. Competing with the overfill/underfill of the nozzle, this mechanism, can be responsible for the flow fields observed at the different frequencies.

To check whether the jetted droplets can induce airflow strong enough to influence the movement of the ink layer more experiments have to be performed. It might be possible to develop a model, which relates the jet of droplets to the movement of the ink layer.

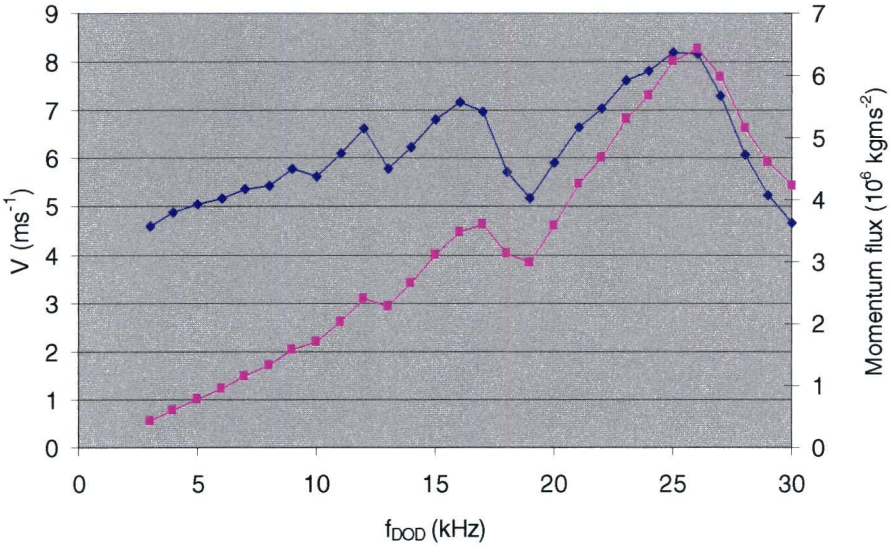

Figure 6.14: Drop on demand speed curve (blue) and the momentum of the stream of droplets (pink) assuming the droplets volume (30 pl) is independent of f_{DOD}.

The experiments with non-jetting pulses (only the meniscus is oscillating and thus no airflow) show steady flow fields in the ink layer. The observed flow fields show a great resemblance with a dipole flow field. The small deviation from the exact dipole flow can be explained by a non-uniform layer thickness as discussed in chapter 4.3.4.
It has to be noted that the dipole fields are always in the same direction as the ink layer thickness gradient.

In chapter 4.5 it is discussed that if capillary waves occur on the nozzle plate a quadrupole like flow field is expected. This makes it quite unlikely that acoustic/micro streaming causes the observed dipole-like flow field or the two directional flow observed at 20 kHz jetting actuation.

It has to be noted that the fluid velocities observed in the sink-like flow and the dipole-like flow are of equal magnitude. From this, it can be understood that the dipole-like field totally disappears when jetting and, vice versa, the sink-like field totally disappears when non-jetting.

Experiments on the transition from dipole to sink like field (and vice versa) have to be performed to get a better understanding of the mechanisms responsible for the observed flow field.

Applying ink to the nozzle plate is a rather inaccurate process. As soon the solid ink touches the hot nozzle plate, it starts to melt and starts spreading. This makes it hard to create a reproducible initial condition. Therefore a method has to be found that makes it possible to define a better start situation.

7. Transitions in flow fields

In the previous chapter it is observed that the flow in the ink layer on the nozzle plate depends both on the frequency and the amplitude of the actuation pulse. It is also pointed out that the flow depends on the wetting conditions at the start.
In this chapter a method is used in which the global wetting of the nozzle plate is decoupled from the local wetting near the nozzle plate. It turns out that this makes it possible to create well defined initial conditions.

7.1 The additional nozzle plate

An additional nozzle plate with a thickness of 25 µm and circular holes of about 500 µm is placed on the existing nozzle plate. The additional nozzle plate is aligned in the way that the nozzles of the existing nozzle plate are exactly at the center of the 500 µm holes of the existing nozzle plate. This is schematically shown in figure 7.1.

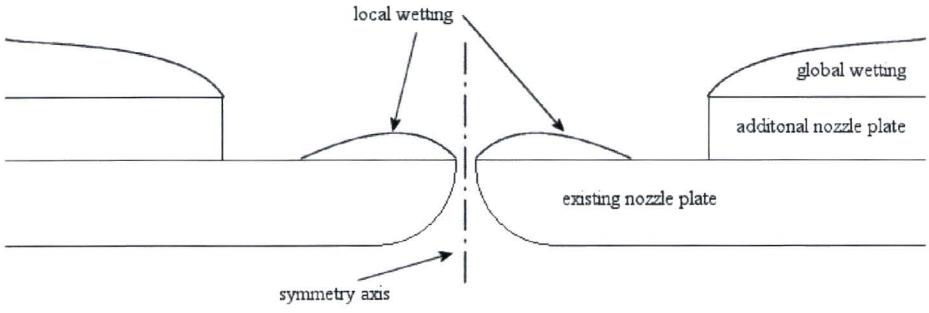

Figure 7.1: Schematic view of the additional nozzle plate on the existing nozzle plate

The abrupt edge of circular hole in the additional nozzle plate causes the contact line to be pinned. This prevents interaction between the global wetting of the nozzle plate and the wetting near the nozzle. In this way the global wetting of the nozzle plate is decoupled from the local wetting conditions near the nozzle.

Since there is no transport from the nozzle plate towards the nozzle and there is a sink flow due to low pressure in the nozzle, the surroundings of the nozzle remain "dry". Only a few Newton rings are visible from which it can be concluded that the layer thickness is a few µm. This causes a well-defined initial condition.

An unpleasant result of this well-defined initial condition is that it is not possible to apply ink with particles to the nozzle plate anymore. As soon as ink with particles is applied near the nozzle the ink is sucked into the nozzle.
This makes it impossible to track particles to calculate flow velocities. It is however possible to determine the sink/source/dipole character of the nozzle by examining the change in contour of the ink layer.
The sink and source flow fields show a circular contour of the ink layer. From the increasing or decreasing radius of the contour it can be concluded whether the flow behaves as a "sink" flow or a "source" flow.

The dipole flow fields show an asymmetric contour of the ink layer: one side of the contour is pulled towards the nozzle. This makes it possible to distinguish the dipolar flow field from the sink or source flow field without using particles.

7.2 Transition from non-jetting to jetting

In chapter 5 it was discussed that the nozzle generally induces a dipole like flow field when non-jetting and a source/sink like flow field when jetting. It was noticed that this behaviour is dependent on the initial conditions of the ink film near the nozzle. Using the additional nozzle plate it is possible to create well defined initial conditions.

The actuation of the piezo is started with a voltage level of about 1V. At this voltage no influence of the nozzle on the ink layer is observed. When slowly increasing the actuation voltage some transitions in the flow field near the nozzle are observed.

At the start voltage of about 1V the surroundings of the nozzle are almost dry due to the low pressure in the head. When increasing this voltage, the nozzle starts to leak ink and after a while a dipole is formed. Further increasing the voltage causes the nozzle to start jetting, in this case the ink layer remains close to the nozzle.
These three different cases are shown in figure 7.2.

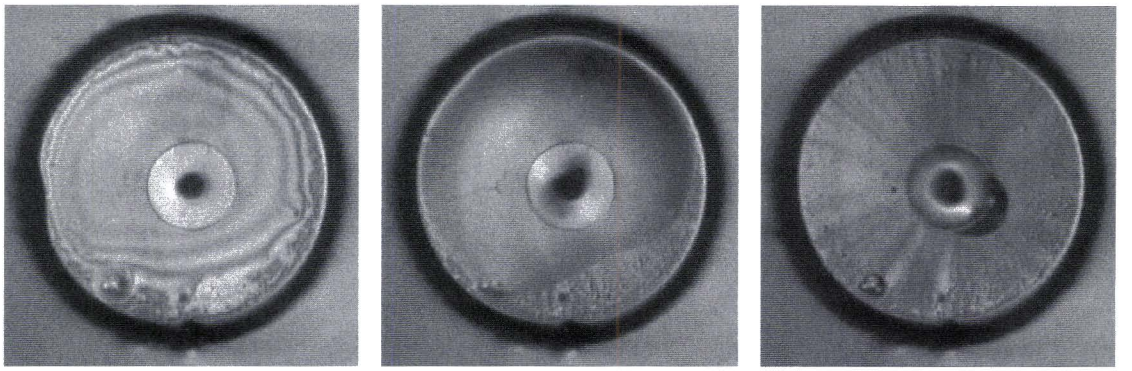

Figure 7.2: Very thin ink layer (a) near the nozzle, which grows to a dipole (b) when increasing the voltage. (c) When the nozzle starts jetting the ink layer remains close to the nozzle.

The voltages at which the transitions occur are determined at the range of 1 kHz to 30 kHz. The results are presented in figure 7.3.

In the orange area of the graph the nozzle has no influence on the ink layer. When the voltage is increased the nozzle starts leaking (green area). The transition voltage from no influence on the ink layer to the leaking behaviour decreases with increasing frequency.

Further increasing the actuation voltage causes another transition in the flow field: a dipole is formed. This is presented as the yellow area in the graph.
It is striking that at frequencies above 19 kHz the nozzle behaves as a sink: just before forming the dipole, the surroundings of the nozzle become dry (blue area).

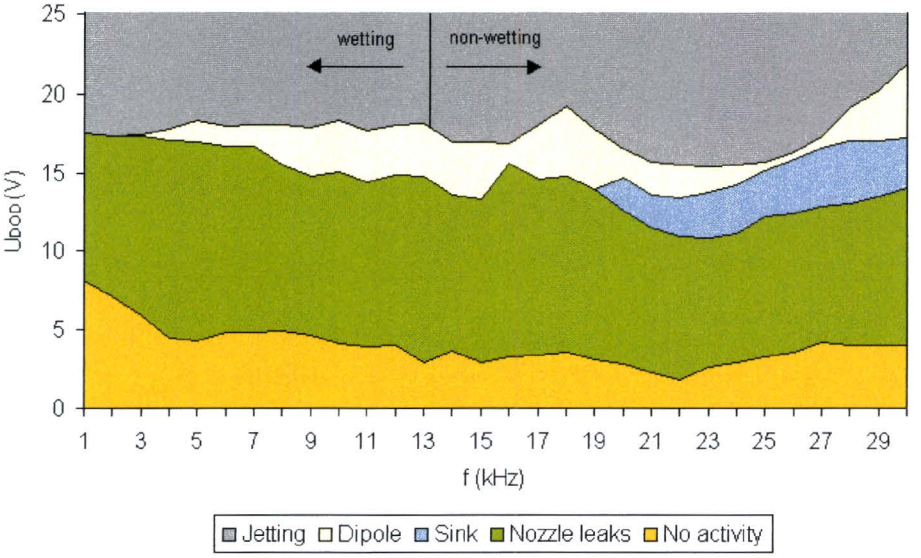

Figure 7.3: Different states of the nozzle depending on the actuation voltage and the DOD frequency.

Further increasing the voltage causes the nozzle to start jetting. At frequencies below 13 kHz the nozzle leaks, at higher frequencies the ink layer remains close to the nozzle.

To get a better picture of the hysteresis in the transition from jetting to non-jetting, this transition is determined when increasing the voltage and the reverse transition, from jetting to non-jetting, is determined when decreasing the voltage. This is presented in figure 7.4.

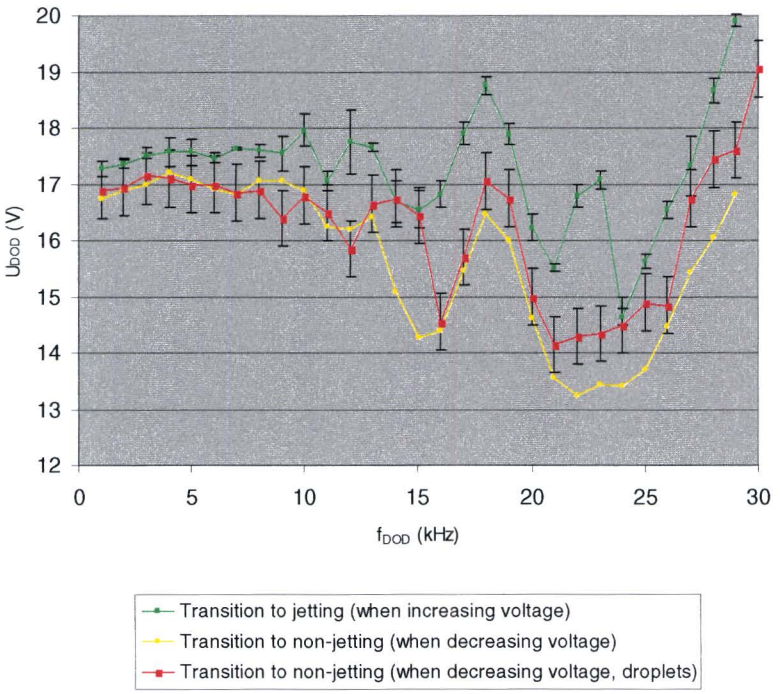

Figure 7.3: The transition from jetting to non-jetting: transitions in flow field.

Figure 7.4 clearly shows that the transition from jetting to non-jetting occurs at a lower voltage than the transition from non-jetting to jetting. This can be explained by the fact that when increasing the voltage first a dipole is formed. This means that there is an ink layer present and a relative high voltage is necessary to jet through this layer. When decreasing the voltage no layer is present, which means that the transition occurs at a slightly lower voltage.

The transition from jetting to non-jetting is also analysed by observing the jetted droplets. The transition voltage is plotted in figure 7.4 (red line).

Figure 7.5 shows a measurement at 20 kHz where the actuation voltage is slowly decreased till the nozzle stops jetting.

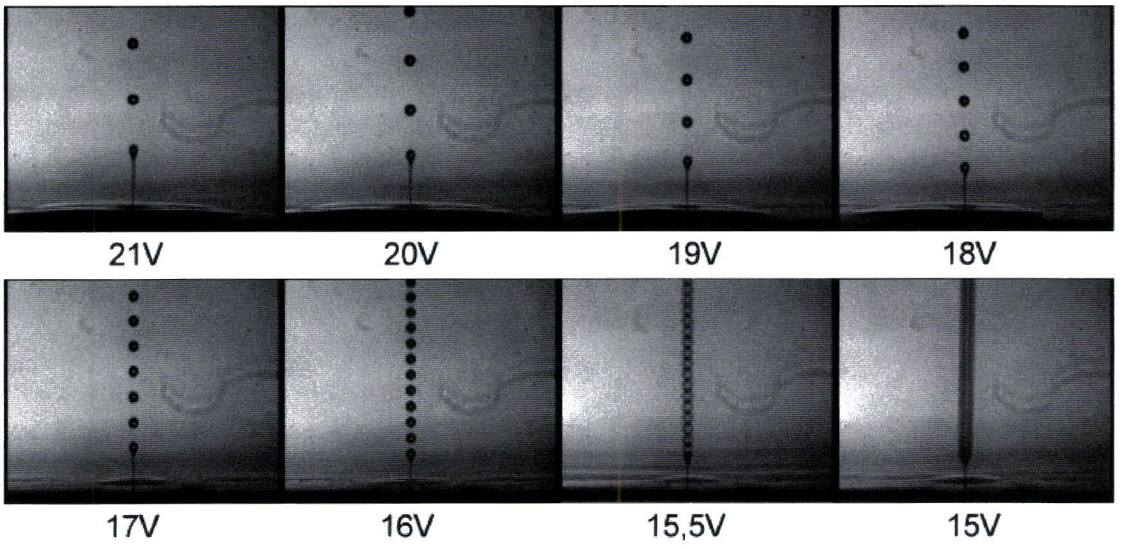

Figure 7.5: Lowering of the jet voltage, just below 15V the nozzle stops jetting at 20 kHz DOD frequency

7.3 Discussion

The measurements show that transitions occur in the flow field when varying the actuation voltage.

At low voltage there is no influence on the layer. The nozzle starts to leak at higher voltages. At the frequency range 1-19 kHz further increasing the voltage causes a transition to a dipole field. At frequencies above 19 kHz a sink like field, which is strong enough to suck up all the ink near the nozzle, precedes the dipole field. When the jetting voltage is reached the final transition occurs. In the final situation the nozzle leaks at frequencies below 13 kHz, at higher frequencies the ink layer is kept close to the nozzle.

At low voltages, below the dipole voltage, the meniscus only vibrates in the nozzle. This causes the nozzle to leak.
At higher voltages, in the dipole regime, the amplitude of the vibration is larger. This probably causes an asymmetry in the nozzle vibration. This subsequently causes the

nozzle to form a dipole: one side of the nozzle functions as a source, while the other side functions as a sink.

At the transition to jetting the meniscus oscillation recovers its symmetric vibration, this causes the dipole to cease to exist. The airflow induced by the train of droplets prevents possible ink from spreading.

The most important difference between the experiments in this chapter (with the additional nozzle plate) and the experiments in chapter 6 (without the additional nozzle plate) is that there is no net transport of ink from the surroundings towards the nozzle. Since there is no ink transport from the surroundings no sink like field (as observed in chapter 6 using jetting pulses) can be maintained. After a period all ink near the nozzle is sucked in the nozzle. At that point it is impossible to determine whether the nozzle still behaves as a sink.

8. Airflow

In the previous chapters it is often discussed that the ink layer on the nozzle plate is influenced by the airflow induced by the jetted droplets. In this chapter first some experiments are performed which prove the airflow. Secondly it is tried to model the airflow.

8.1 Experiments

In this chapter some experiments are performed which prove that there is an airflow present and that this airflow is able to influence the motion of the ink layer.
First the airflow is visualised using a streak of smoke. Also its influence on crossing droplets is determined. Secondly the influence of the airflow on a layer of ink is visualised.

Smoke is used to visualize the airflow. The smoke is applied close to the nozzle using an injection needle.
Figure 8.1 shows a jet of droplets and a horizontal streak of smoke coming from the right. Because the dimensions of the streak of smoke are large compared to the dimensions of the jet of droplets most of the streak moves in the front and in the back past the jet. The jet influences a small part, which shows as the vertical streak of smoke at the right of the jetted droplets in figure 8.1.

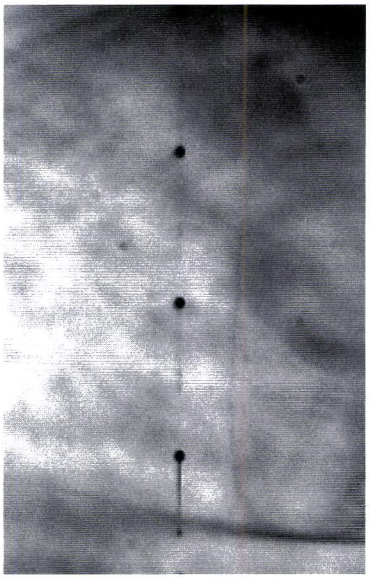

Figure 8.1: A streak of smoke is used to visualise the airflow

The streak of smoke is bent at a distance of about 200 µm from the jet. This clearly shows that there is airflow present and gives an indication of the region of influence of the jet.
The apparent movement of the streak of smoke can not be used to calculate the speed of the airflow since it represents both the movement of the streak in the depth of the picture and the motion of the streak due to the airflow induced by the droplets.

Another proof of the airflow is observed with the high-speed camera (100.000 frames per second). Figure 8.2 shows droplets, moving in horizontal direction along the jet, that are bent towards the jet direction. It is clearly visible that particles close to the nozzle (sharp) are bent more than particles far from the nozzle (un-sharp).

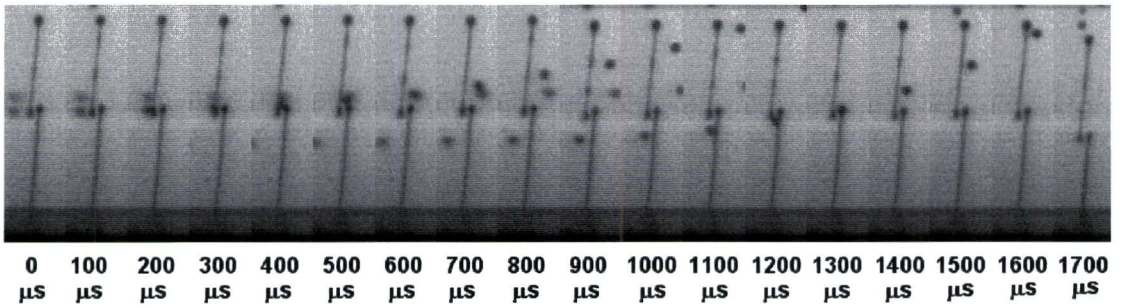

Figure 8.2: The airflow caused by the drop formation process causes horizontal moving droplets to be bent towards the jetting direction.

By further analysing the flow it is determined that the droplets move with a horizontal velocity of about 0,1 m/s. Within 1 ms the droplets is accelerated from a zero vertical velocity to a vertical velocity of about 1 m/s. From this it can be concluded that the air through which the droplets moves has a velocity more than 1 m/s and probably close to the velocity of the jetted droplets.

To prove that the generated airflow influences the movement of the ink layer the setup with the additional nozzle plate is again used. Instead of focussing on the ink flow near the nozzle (on the existing nozzle plate), we focus on the ink flow on the additional nozzle plate.
Ink with particles is applied to the additional nozzle plate. When the ink touches the nozzle plate it starts spreading. After a while the movement of the ink layer comes to rest and jetting is started.
Since the ink on the additional nozzle plate has no contact with the nozzle, its movement can only be influenced by a present airflow. The observed movement of the ink layer is analysed with the PTV script and presented in figure 8.3.

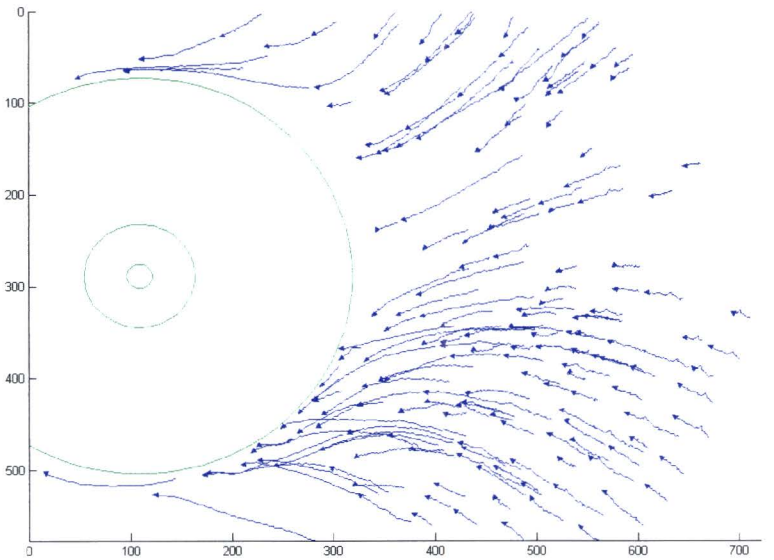

Figure 8.3: particle lines of the flow on the additional nozzle plate. Scales in pixel (1 pix ≈ 1,2 µm)

Figure 8.2 clearly shows a movement of the ink layer towards the nozzle although there is no fluid contact between the nozzle and the ink layer. Further analysis shows that there is no clear r-dependence in the velocity. This is probably caused by a piling up of ink and particles at the edge of the additional nozzle plate. This disturbs the movement of the ink layer causing it to deviate from the common sink link behaviour.

It is clear that the jetted droplets induce an airflow, which subsequently influences the movement of the ink layer. It is also apparent that in order to get a sink like behaviour of the nozzle there has to be ink contact between the nozzle and the ink layer.

8.2 Modelling the airflow

8.2.1. Momentum transfer by a single droplet

Friction causes a droplet that moves through the air to slow down. The droplet is decelerated from its original velocity v_1 to zero. The loss in momentum is transferred to the surrounding air. This causes the air to accelerate.

The momentum equation for one droplet is given by:

$$m\frac{Dv_d}{Dt} = -2\pi r_d \mu Nu_F v_d . \tag{8.1}$$

With the Nusselt number for momentum transfer defined by [NAU33]:

$$Nu_F = 3(1+0.15\mathrm{Re}_d^n) \text{ with n} = 0.687 \tag{8.2}$$

The time derivative in equation (8.1) refers to "particle time", and is for steady flow related to the spatial derivative by:

$$\frac{D}{Dt} = v_d \frac{d}{dx} . \tag{8.3}$$

Equation (8.1) and (8.2) can be solved. The result can be expressed as a time dependence of the Reynolds number $\hat{\mathrm{Re}}_d = 2r_d v_d / \nu_{air}$, starting from the initial value $\hat{\mathrm{Re}}_{d1} = \hat{\mathrm{Re}}_d(v_d = v_1) = 2r_d v_1 / \nu_{air}$:

$$t = \frac{2}{9}\frac{\rho_{ink} r_d^{\,2}}{\mu_{air}} f(\hat{\mathrm{Re}}_d ; \hat{\mathrm{Re}}_{d1}) \tag{8.4}$$

$$f(\hat{\mathrm{Re}}_d ; \hat{\mathrm{Re}}_{d1}) = \ln\frac{\hat{\mathrm{Re}}_{d1}}{\hat{\mathrm{Re}}_d} + \frac{1}{n}\ln\frac{1+0.15\hat{\mathrm{Re}}_d^n}{1+0.15\hat{\mathrm{Re}}_{d1}^n} \tag{8.5}$$

Using equation (8.4) and (8.5) it is possible to calculate the trajectory of a single droplet of ink with a radius of 15 µm and an initial velocity of 6 m/s.

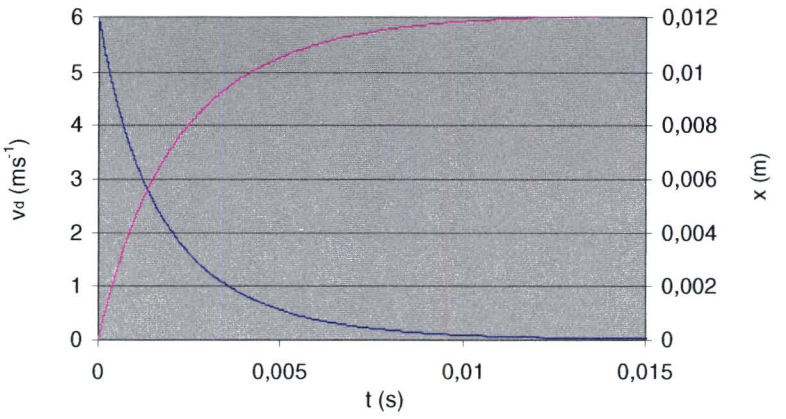

Figure 8.4: Droplet speed (blue) and droplet distance (pink) from the nozzle (x) as a function of time.

The momentum lost by the droplets is transferred to the air. While the droplets move a distance dx through the air they exert a force (per length unit) which is equal to the loss of momentum, neglecting interaction between droplets:

$$F_x dx = f_{DOD} m v_d\big|_x - f_{DOD} m v_d\big|_{x+dx}. \tag{8.6}$$

This can be written as:

$$F_x = -f_{DOD} m \frac{dv_d}{dx} \tag{8.7}$$

By applying (8.3) this can be written as:

$$F_x = -f_{DOD} m \frac{1}{v_d} \frac{Dv_d}{Dt} = 2 f_{DOD} \pi r_d \mu Nu_F \tag{8.8}$$

This equation can numerically be solved. This force per length unit can be converted to a volume force by assuming that the force is applied in a circular area with the nozzle radius. Next this force distribution can be used as an input for a numerical package to calculate the entire flow field.

The momentum transfer for a train of droplets with mutual interaction, which will be discussed in the next chapter, is more complex.

8.2.2. Momentum transfer by a train of droplets

Lee [LEE76] describes the boundary layer of air induced by a train of droplets. In a train of droplets, the trapped air between closely spaced drops moves with the droplets and inhibits the development of an axial pressure gradient, making the skin friction more significant than the form drag. This makes it possible to replace the droplets with an equivalent section of cylindrical shapes.

The rate of momentum transfer from the cylinder to the boundary layer through skin friction varies along the axial co-ordinate because the transfer causes the jet to slow down, resulting in growth of the cross section of the jet.

The momentum and continuity equations applied to a boundary layer of thickness δ and a liquid jet of radius a are:

$$2\pi\rho_a \int_0^{\delta(x)} [a(x)+y]v^2(x,y)dy + \rho_l \pi a^2(x) v_l^{\,2}(x) = \rho_l \pi a_0^{\,2} v_{l0}^{\,2} \tag{8.9}$$

$$\frac{d}{dx}[\pi\rho_l a^2(x) v_l^{\,2}(\bar{x})] = 2\pi a(x)\mu_a \left.\frac{\partial v}{\partial y}\right|_{y=0} \tag{8.10}$$

$$\pi a^2(x) v_l(x) = \pi a_0^{\,2} v_{l0} \tag{8.11}$$

The co-ordinate x is in the jet direction, and y is measured radially from the surface of the liquid jet (as shown in figure 8.5).
Velocity, density and viscosity are denoted by ν, ρ and μ, respectively, with the subscripts a and l for air and ink, respectively. The subscript 0 denotes the initial values at the nozzle.

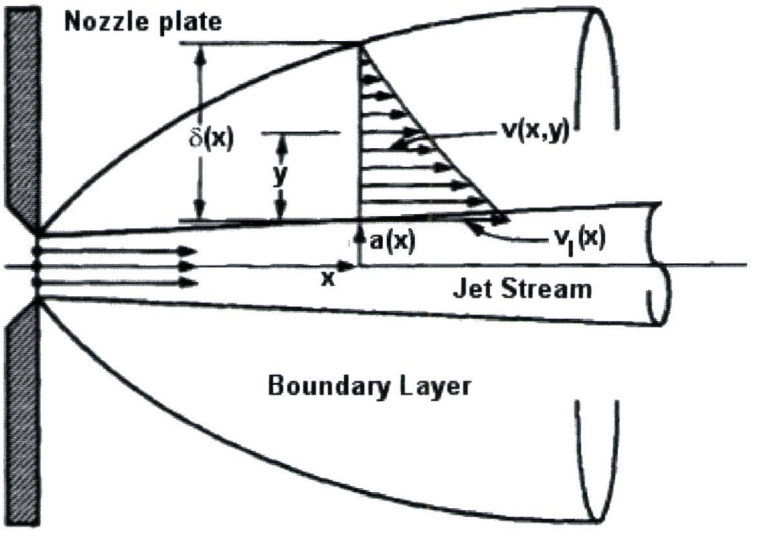

Figure 8.5: Boundary layer induced by a jet emerging from a nozzle

Equation (8.9) represents the conservation of axial momentum. Equation (8.10) matches the rate of momentum loss to the skin friction of the jet. Mass conservation, or the continuity of the liquid jet, is expressed in equation (8.11).

An approximate solution for the boundary layer equation in integral form can be obtained by assuming a velocity profile of the airflow in the boundary layer that satisfies the boundary conditions:

$$v(x,0) = v_l(x), \tag{8.12}$$

$$\left[\frac{\partial^2 v}{\partial y^2} + \frac{1}{a}\frac{\partial v}{\partial y}\right]_{y=0} = 0, \tag{8.13}$$

$$v(x,\delta) = 0. \tag{8.14}$$

Equations (8.12) and (8.14) require the x-component of the air velocity to be zero at the outer boundary and equal to the liquid velocity at the interface. Equation (8.13) is the result of applying the differential momentum equation at the interface boundary but away from the nozzle.

A logarithmic velocity profile would be appropriate:

$$v(x,y) = v_l(x)\left\{1 - \frac{1}{\beta(x)}\ln\left[1 + \frac{y}{a(x)}\right]\right\}, \tag{8.15}$$

where

$$\beta(x) = \ln\left[1 + \frac{\delta(x)}{a(x)}\right]. \tag{8.16}$$

The boundary problem is solved by substitution of equation (8.15) in equations (8.9-11). Elimination of a results in:

$$\bar{v}_l(x) = \frac{v_l(\bar{x})}{v_{l0}} = \frac{1}{1 - \bar{\rho}\left[1 + \frac{1}{\beta} - \frac{1}{2\beta^2}(e^{2\beta} - 1)\right]}, \tag{8.17}$$

$$\frac{d\bar{v}_l}{dz} = -\rho\frac{\bar{v}_l(\bar{x})}{\beta(\bar{x})}, \tag{8.18}$$

or by substituting equation (8.17) in (8.18):

$$\frac{d\beta(\bar{x})}{d\bar{x}} = \frac{\beta^2 - \bar{\rho}[\beta^2 + \beta - \frac{1}{2}(e^{2\beta} - 1)]}{\beta(1 + e^{2\beta}) - (e^{2\beta} - 1)}. \tag{8.19}$$

where

$$\bar{x} = \frac{4}{\mathrm{Re}}\frac{x}{a_0}, \text{ with } \mathrm{Re} = \frac{2a_0 v_{l0}}{\upsilon_a} \text{ and } \bar{\rho} = \frac{\rho_a}{\rho_l} \tag{8.20}$$

Lee calculates the velocity decrease of the stream of droplets by numerically integrating equation (8.16) using a finite difference method. This is shown in figure 8.7.

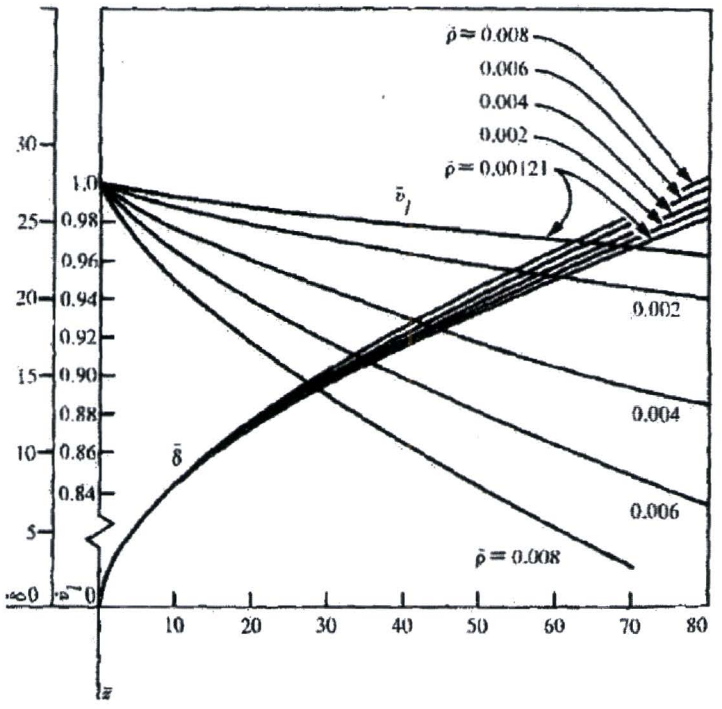

Figure 8.6: Stream velocity and boundary layer thickness for various values of density ratio.

The entrainment of air by the jet can be expressed as the derivative to x, of the flux of air through the boundary layer:

$$q(x) = 2\pi \frac{\partial}{\partial x}\left[\int_0^{\delta(x)} v(x,y)dy\right] \tag{8.21}$$

It is tried to calculate the entire flow field by placing sources of strength q(x) along δ(x). By integrating over the sources the total flow field can be obtained. In order to perform this calculation it is necessary that the behaviour of the boundary layer for $x \downarrow 0$ and $x \to \infty$ is known.

When checking Lee's derivation of equation (8.17) another result for equation (8.17) is obtained. When numerically integrating equation (8.19) and calculating the boundary layer thickness it seems that the boundary layer has diverging properties for higher x values (not shown in Lee's article). This makes it impossible to get a result for the entire flow field.

This is why we abandon Lee's description and move to the well-known problem of the circular laminar jet.

8.2.2. The laminar jet

A well-known problem, solved by Schlichting [SCH60], is that of a circular laminar jet in which a constant momentum flux is assumed. For large distances from the nozzle, this is a reasonable approximation for the airflow induced by the train of droplets.

A jet which leaves a small circular opening and mixes with the surrounding fluid. The pressure is regarded as constant. Because of the assumption that the pressure is constant, the flux of the momentum in the direction of x is constant:

$$J = 2\pi\rho\int_0^\infty u^2 y dy = const. \tag{8.22}$$

The system of co-ordinates is chosen with the x-axis in the axis of the jet, the radial distance is denoted by y.

Under the usual boundary-layer simplifications the equation of motion in the direction of x can be written as:

$$u\frac{\partial u}{\partial x} + v\frac{\partial u}{\partial y} = \nu\frac{1}{y}\frac{\partial}{\partial y}\left(y\frac{\partial u}{\partial y}\right), \tag{8.23}$$

$$\frac{\partial u}{\partial x} + \frac{\partial v}{\partial y} + \frac{v}{y} = 0. \tag{8.24}$$

The boundary conditions are:

$$y = 0:\ v = 0,\ \frac{\partial u}{\partial y} = 0. \tag{8.25}$$

$$y = \infty : u = 0. \tag{8.26}$$

The velocity profiles $u(x,y)$ can be assumed similar. By following Schlichting's derivation [SCH60] the velocity field can be expressed in the kinematic viscosity, ν, and the kinematic momentum $K' = J/\rho$:

$$u = \frac{3}{8\pi}\frac{K'}{\nu x}\frac{1}{(1+\frac{1}{4}\zeta^2)^2} \tag{8.27}$$

$$v = \frac{1}{4}\sqrt{\frac{3}{\pi}}\frac{\sqrt{K'}}{x}\frac{\zeta - \frac{1}{4}\zeta^3}{(1+\frac{1}{4}\zeta^2)^2} \tag{8.28}$$

$$\zeta = \sqrt{\frac{3}{16\pi}}\frac{\sqrt{K'}}{\nu}\frac{y}{x} \tag{8.29}$$

Figure 8.7 represents the streamline pattern calculated from equation (8.27) through (8.29).

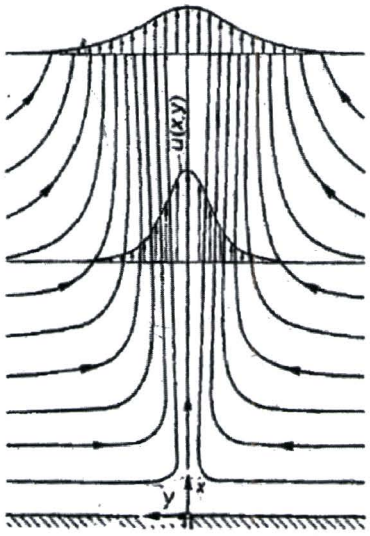

Figure 8.7: Streamline pattern for a circular laminar jet

The volume of flow, which increases with the distance from the orifice due to the flow from the surroundings, is represented by the simple equation:

$$Q = 2\pi \int_0^\infty uydy = 8\pi\nu x \tag{8.30}$$

It is seen that the volume flow at a given distance, x, is independent of the momentum of the jet. A jet that leaves at large velocity remains narrower than a jet leaving at small velocity. The latter carries with it comparatively more stationary air.

8.2.3. Influence on the ink layer

In the previous section it is shown that a laminar jet, and thus also a jet of droplets, induces an airflow towards the nozzle (y=0). The airflow exercises a force on the top of the ink layer on the nozzle plate, causing the ink layer to move towards the nozzle.

The horizontal velocity component of the airflow induced by the laminar jet can be calculated by substituting equation (8.29) in (8.28):

$$v(x,y) = 12\frac{\nu Ky(64\pi\nu^2 x^2 - 3Ky^2)}{(64\pi\nu^2 x^2 + 3Ky^2)^2} \tag{8.31}$$

The velocity of the airflow over the nozzle plate is calculated by taking the limit x ↓ 0 of equation (8.31):

$$v_s(y) = \lim_{x\downarrow 0} v(x,y) = -4\frac{\nu}{y} \tag{8.32}$$

The solution shows an *1/y* dependency which is also found in the experiments. It is striking that the velocity of the airflow over the nozzle is independent of the momentum of the jet. This is probably caused by the fact that at x=0 the nozzle is proposed as a point source of momentum.

Since the solution for the air flow near the nozzle plate does not take into account viscosity it is impossible to calculate the influence of the airflow on the ink layer by calculating the stress the airflow exerts on the ink layer. In order to do this a boundary layer model for the airflow over the nozzle plate needs to be developed.

8.3 Flow 3d

Flow3d (9.0) is a CFD program, which is used to simulate the drop formation process, using a specified nozzle shape, from a specified pressure input on the nozzle. A well chosen mesh is very important for a successful simulation.

Using Flow 3d it has been tried to simulate the influence of the droplets on the airflow. An existing, cylinder symmetrical model is modified to calculate the influence of the jetted droplets. A second fluid is added with the properties of air (figure 8.9). The horizontal size of the simulation domain is increased to a radius of 225 µm.

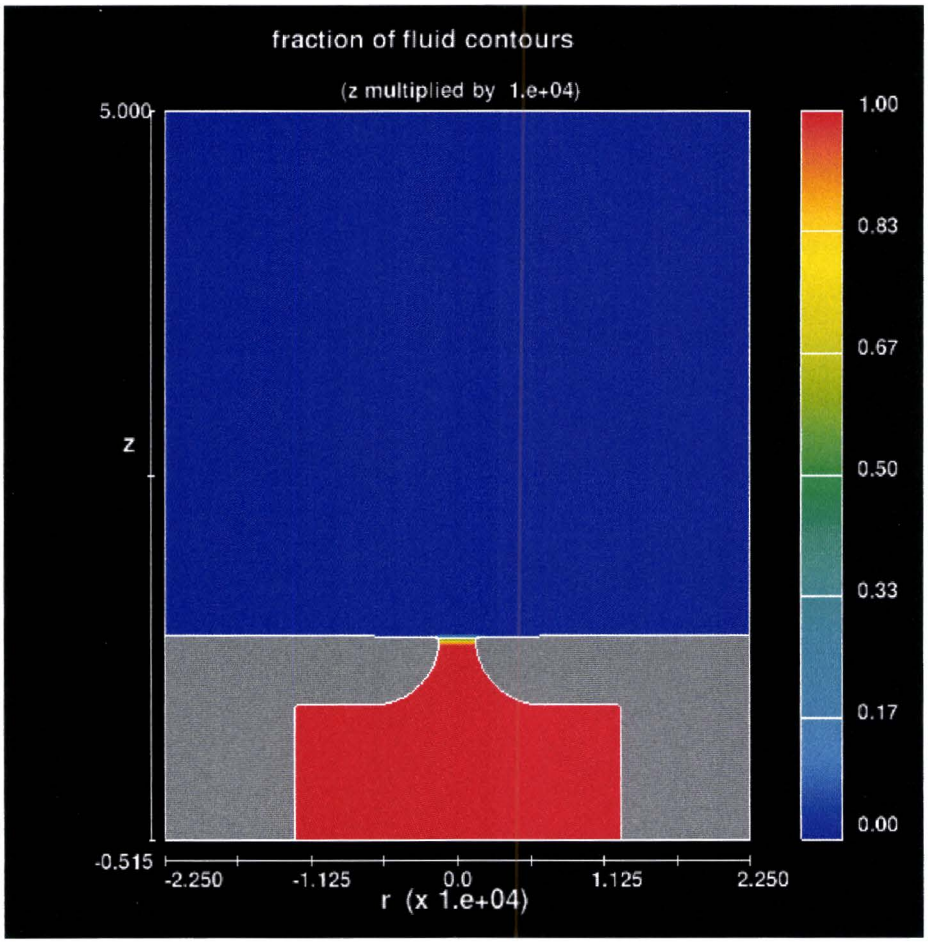

Figure 8.9: The two fluid model used in Flow 3D. Red indicates ink and blue indicates air.

The boundary conditions are:

x_{min}: symmetry plane,
x_{max}: specified pressure (ambient pressure),
z_{min}: specified pressure (stagnation pressure, from acoustic model),
z_{max}: outflow.

Choosing a coarse grid makes it possible to calculate the formation of eight successive droplets and their influence on the airflow. The simulation clearly shows air coming from the boundaries.

Upon further investigation it turns out that Flow 3D only calculates one velocity in each computational cell. When the densities of the two fluids differ greatly, this velocity can not represent the flow, since the velocities of each of the fluids in the same cell may be very different. As a consequence slip conditions between the fluids are not modelled accurately, which results in an incorrect fluid interface motion. Flow Science has been contacted for a possible solution to this limitation.

Since the density of the air is about a factor 1000 times smaller than the density of the ink, it is not possible to use Flow 3d's 2 fluid model to simulate the influence of the droplets on the airflow.

8.4 Discussion

The experiments in the beginning of this chapter clearly demonstrate that the jet of droplets induces airflow, which subsequently is strong enough to cause movement of the ink layer towards the nozzle.
The experiment with the additional nozzle plate clearly shows that it is very important that there is ink contact between the nozzle and an ink layer on the nozzle plate in order to get the typical sink like nozzle behaviour.

To get a more quantitative picture of the velocity magnitude of the airflow and the subsequent velocity magnitude of the ink layer it is tried to develop a model, which relates the DOD frequency to the amount of airflow.

During the literature study it appeared that very little is known on the problem of a train of droplets moving through air and the airflow it induces.
Lee's article [LEE76] gives a description of the impulse loss for a train of droplets moving through air. When tracking his derivation and extending it for the total airflow induced by the train of droplets it turns out that the solution has diverging properties making it impossible to calculate the total flow field.

Finally a laminar jet replaces the train of droplets. For large distances from the nozzle, this is a reasonable approximation for the airflow induced by the train of droplets. Calculations show an 1/r dependency of the speed of the airflow over the nozzle plate.

9. Nozzle plate vibration

Using speckle interferometry it is checked whether the actuation of the piezo causes vibrations in the nozzle plate.

9.1 Theory

Speckle interferometry is based on the principle that a diffuse reflection of coherent laser light on a rough surface leads to a speckle pattern caused by interference. When the surface roughness is larger than the wavelength of the used light the surface behaves as a plane of point sources.
Phase shifts due to the movement (parallel to the laser beam) of the rough surface can be measured by letting the speckles interfere with a reference laser beam.
By measuring the intensity of the composed beam as a function of the position on the surface it is possible to determine the displacement of the entire surface in time.
The used experimental setup is shown in figure 9.1.

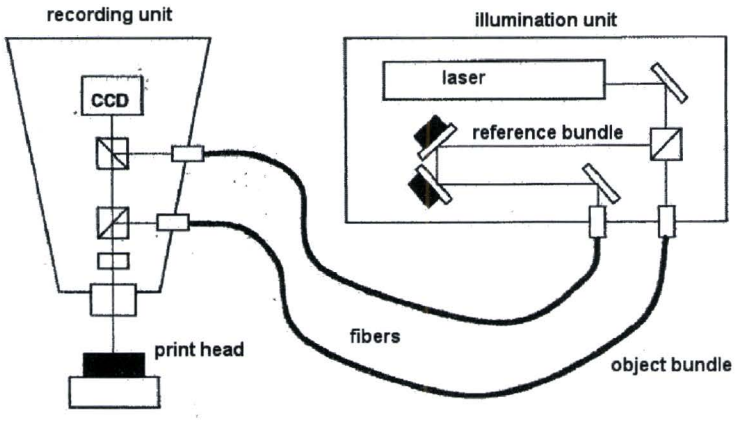

Figure 9.1: schematic experimental setup of the Speckle interferometer

Figure 9.1 shows the illumination unit, which contains the laser for the coherent light and a beam splitter and mirrors to create the object beam and the reference beam.
Using fibers, the two light beams are transferred to the recording unit. The reference unit is transferred directly to the CCD camera, the object beam is first reflected on the nozzle plate and then transferred to the CCD camera. On the CCD the two beams interfere [FRB].

9.2 Experiments

The schematic setup in picture 9.1 shows that the nozzle plate side of the ink head must be face up in order to perform measurements using the Speckle interferometer. To prevent ink from leaking from the head when turned upside down, the head is maintained at room temperature, which causes the ink to be in solid form.

The solid ink in the ink channels contains a lot of air bubbles. These air bubbles prevent the transport of additional vibrations from the piezo towards the nozzle plate through the solid ink.

Experiments are started with a measurement to determine the noise level of the measuring method. Measuring the displacement of the nozzle plate when no piezos are actuated does this. The result is presented in figure 9.2.

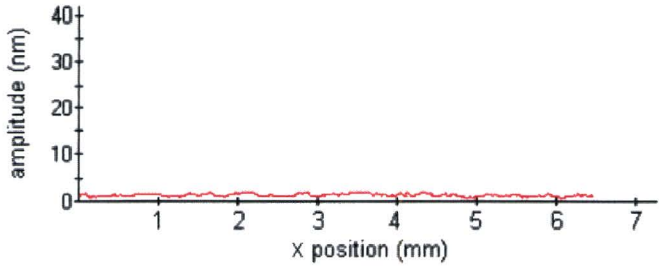

Figure 9.2: Scan in the x-direction of the nozzle plate showing the absolute amplitude of the vibration.

After determining the noise level of the measuring method, measurements were started during which a single piezo finger was continuously actuated with a sine pulse. No influence on the displacement of the nozzle plate was measured.
To obtain a notable displacement of the nozzle plate 60% of the piezo fingers at one side (x=0) of the array were actuated. The results are presented in figure 9.3

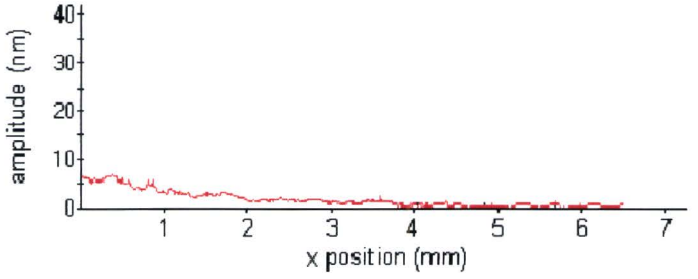

Figure 9.3: Scan in the x-direction of the nozzle plate showing the absolute amplitude of vibration when actuating 60% of the piezo fingers at y=0.

The amplitude of motion in 9.3 is noticeable higher than the noise level (figure 9.2). From this we can conclude that the actuation of the piezo fingers causes a vibration in the nozzle plate.

9.3 Discussion

It can be concluded that there is an influence of the piezo fingers on the movement of the nozzle plate. Actuating a large part of the piezo fingers at one side of the nozzle plate causes a transversal movement of the nozzle plate. Actuating one piezo finger however does not cause any measurable motion.
The maximum measured amplitude of the vibration of the nozzle plate is about 5 nm. Since this amplitude is much less than the ink layer thickness (25 µm) it is very unlikely that it influences the ink flow on the nozzle plate. It is possible that this vibration can cause capillary waves which subsequently can cause flow fields on the nozzle plate by microstreaming.

10. Conclusions and discussion

10.1 Conclusions

Under practical print conditions, there is always an ink layer present on the nozzle plate of the checked printheads. This agrees with the small contact angle ($\theta < 20°$).
It is not possible to wipe off the entire ink layer, always a very thin (few micron) ink layer remains present. The nozzle plate only dries up after waiting a long period of time while the printhead is inactive.

Jetting actuation pulses cause sink/source-like flow fields on the nozzle plate.
The driving forces behind the flow fields observed on the nozzle plate are surface tension and in case of jetting friction with airflow induced by the jetted droplets.
Analysis shows that the flow in the ink layer on the nozzle plate can be approximately described by 2D potential flow. Small deviations are found due to the non-uniform layer thickness.

Experiments show a flow of ink towards jetting nozzles. This transport can cause dirt particles, which are caught in the ink layer on the nozzle plate, to reach the nozzle and cause instability.

At 20 kHz the jetting nozzle causes a two directional radial flow field. This can be explained by the fact that the nozzle behaves as a source of ink. The surface tension acts as a driving force, causing the ink to flow from the nozzle. Together with the movement of the airflow towards the nozzle, this results in the two-directional flow field observed in the ink layer.

Experiments on a nozzle with initially dry surroundings show that the nozzle leaks at frequencies below 13 kHz.
At higher frequencies the surroundings of the nozzle remain dry. This is in contradiction with the two directional flow observed at 20 kHz. This is not understood.

Non-jetting actuation pulses show a variety of flow fields, depending on the amplitude. For voltages below about 4V the nozzle shows no influence on the surroundings. At higher voltages the nozzle leaks. At a voltage just below the transition voltage from non-jetting to jetting a dipole-like flow field is observed, which subsequently disappears when the voltage is increased to jetting level.

The mechanism behind the dipole field remains unknown. Since the direction of the dipole is always along the ink layer thickness gradient, it is expected that non-uniform wetting conditions near the nozzle cause an asymmetrical movement of the meniscus.

10.2 Discussion

At high frequencies, airflow is an important mechanism for transport towards the nozzle. The airflow makes it possible that a jetting nozzle is able to exercise a force on an ink layer without having fluid contact with the ink layer.

This can cause the ink layer to move to a neighbouring nozzle. At the critical layer thickness this can cause an air bubble.
It has to be kept in mind that the ink layer on a printhead in a moving carriage, not only experiences a force due to the acceleration of the carriage (inertia), but also due to an additional airflow caused by the movement of the carriage. This is an additional cause of ink layers flowing over nozzles.

In order to prevent particles from reaching the nozzle by transport in the ink layer it is best to avoid the presence of an ink layer on the nozzle plate.
Experiments have however shown that it is hard to prevent an ink layer on the nozzle plate under practical print conditions:
1. Jetting nozzles at frequencies below 13 kHz show leakage
2. Non-jetting nozzles are very sensitive to leakage. A slight actuation, even caused by cross talk from a jetting neighbour nozzle, can cause them to leak.

From this it can be expected that, when starting with a dry nozzle plate, the nozzle plate will remain dry when all nozzles are jetting at a DOD frequency above 13 kHz. When some nozzles are non-jetting, crosstalk will cause them to start leaking. This results in an ink layer, which, at a critical layer thickness, can cause nozzle failure.
At DOD-frequencies below 13 kHz always an ink layer is formed. Since the drop formation at low frequencies is less sensitive for air bubble (formation) this will cause less nozzle failure than an ink layer at high frequencies.

Instead of preventing an ink layer on the nozzle plate it is possible to control the behaviour of the ink layer on the nozzle plate. It could be possible to use a nozzle plate with poor wetting conditions. This prevents the formation of an ink layer and subsequently the transport of particles towards the nozzle.

11. Literature

General Literature

AND32 E.N. da C. Andrade
Proc.Roy Soc. A. 134, 1932.

FTV1 Fysische Transportverschijnselen Deel 1
P.P.J.M. Schram, G.J.F. van Heijst, M.E.H. van Dongen
Eindhoven, 1994

HEI98 Acoustisch Refill-mechanisme in een piëzo inkjetkop
J. v.d. Heijden
Master Thesis, TU/e Eindhoven, 1998

HIL03 Controlled vesicle deformation and lysis by single oscillation bubbles
Philippe Marmottant & Sascha Hilgenfeldt
Nature, Vol 423, 2003

JON03 Air entrapment in piezo-driven inkjet printheads
Jos de Jong
Master Thesis, Universiteit Twente, 2003

KAM95 Acoustic streaming induced in focussed gaussian beams
T. Kamakura, K. Matsuda, Y. Kumamoto and M.A. Breazeale
J. Acoust. Soc. Am. Pp 2740-2746, 1995.

LEE76 Boundary Layer Around A Liquid Jet
H.C. Lee
IBM J.Res.Develop., 1976.

LEI94 The acoustic bubble
T.G. Leighton
Academic Press, London 1994

MID95 Modelling Axisymmetric Flows
Stanley Middleman
Academic Press, San Diego 1995

MIT98 The mechanism of generation of acoustic streaming
Hideto Mitome
National Industrial Research Institute of Nagoya, 1998

NAU33 Ueber die grundlegenden Berechnungen bei der Schwerkraftaubereitung
L. Schiller & A. Naumann
Z. Ver. Deut. Ing. Vol 77, 1933

SCH60 Boundary Layer Theory
Herman Schlichting
McGraw-Hill Book Company, 1960.

Océ Internal Reports

MVDB Marc van den Berg
FRB Frans Blom

Appendix A: Apparatus

PC
The PC is used to control the printhead. It programs the pulse that is put on the piëzo, activates the nozzles and controls the motion of the printheads. This is done by Labview programs. The PC is connected to the different apparatus by GPIB.
The PC is also used for capturing the video stream from the camera. Capturing is done at a resolution of 720 x 576 pixels at 25 frames per second.

Philips PM5150
Two of these waveform generators are used in this setup. The first device is used to control the frequency of the jetting process. The second waveform generator is switched as a slave and delivers a pulse when the first waveform generates a trigger. Using the two waveform generators it is possible to manually control the pulse amplitude and frequency on the fly. The pulse shape is programmed using the PC.

LSA
This is a regular amplifier, which amplifies the actuation pulses. It has four different channels and has an amplification of ten times. This apparatus is needed because high voltages have to be offered to the piezo.

Switchboard
The switchboard consists of a high number of relais. Each relais is used to control one ink channel. The PC determines which relais are open and which are closed. When a relais is open the actuation pulse is transferred to the piezo. Because the piezo must have positive voltages to prevent depolarisation an offset of 45 Volt is set on the board.

Motion System
This system from Newport consists of a driver module, the MM4005 and two actuators (Newport 850F). This apparatus controls the movement of the printhead. The motion controller is controlled by Labview.

Pressure regulator
The EFD 1500XL is a pressure controller which is used to offer a constant negative pressure (compared to ambient pressure) to the ink head. This prevents the nozzles from leaking.

Temperature controller
The temperature controllers are used to control the temperature of the nozzle plate and the melting unit. Both are at a different temperature.

This is the standard setup. Two optical systems are available, one to visualize the jetting behaviour and one to visualise the nozzle plate.
The system to visualise the jetting behaviour consists of a LED connected to the Philips wavegenerator. This LED is flashing at the DOD frequency. The pulse length of the LED is 300ns. It is used to create a stroboscopic image on the camera.

The system to visualise the nozzle plate uses a cold light source to perpendicularly light the nozzle plate via a mirror.

LED
The LED is a TLRH190P from Toshiba. It is a red LED with a wavelength of 650 nm and a small angle of 4 degrees.

Cold Light Source
The Olympus Highlight 3100 is used for illuminating the nozzle plate. The light source is connected to the Olympus stereo microscope.

Mirror
A $1cm^2$ square mirror is placed between the microscope and the nozzle plate to perpendicularly light and visualise the nozzle plate.

Olympus stereomicroscope
The microscope consists of several modules. First the light enters through the objective. There are two different objectives available: one that magnification one time and one that magnifies two times. After the objective is a magnification module which can magnify up to 7 times (0,7, 1, 1,5, 2, 2,5, 3, 4, 5, 6 and 7). The light then passes through the photo tube to the camera.

Camera
The camera is connected to the stereomicroscope. Two cameras where available: the Sony SSC-C370 and the Watec LCL 902K. An extensive comparison is given in Appendix B.

Appendix B: Camera Comparison

Measurements with small angle lighting indicate that the Sony SSC-C370 camera is not very capable of detecting the small amount of light scattered from the particles. Table B1 shows the specifications of both the Sony and the Watec camera. In this chapter the performance of the Sony SSC-C370 is compared to the performance of the Watec LCL 902K.

Table B1: Specifications

	Sony SSC-C370	**Watec LCL 902K**
Pick-up device	CCIR	CCIR
Sensing Area	6,3 x 4,7 mm ($^1/_4$ x $^3/_{16}$ Inch)	$^1/_2$ Inch
Effective pixels (H x V)	752 x 582	752 x 582
Cell size (µm)	8,4 x 8,1	8,6 x 8,3
Minimum illumination	0.3 lx at F/1.2 (AGC on)	0,00015 LX at F/1.4 (AGC high) 0,0015 LX at F/1.4 (AGC low)
S/N Ratio	50 dB minimum (AGC off)	More than 50 dB (AGC off)
Shutter speed	1/50 s , 1/120 s, 1/250 s, 1/500 s, 1/1000 s, 1/4000 s, 1/10000 s	1/50, 1/120 s, 1/250 s, 1/500 s, 1/1000 s, 1/2000 s, 1/5000 s, 1/10000 s, 1/100000 s

B1. Measurements

Table B1 suggests that the Watec camera is the most sensitive camera. Experiments are performed to check the performance of both cameras in an experimental setup.

Figure A1 shows two snapshots (and the corresponding histogram) of the same position on the nozzle plate. The left snapshot is obtained with the Sony camera, the right with the Watec camera. Both snapshots are obtained with the auto gain off and the maximal magnification of the Olympus microscope.

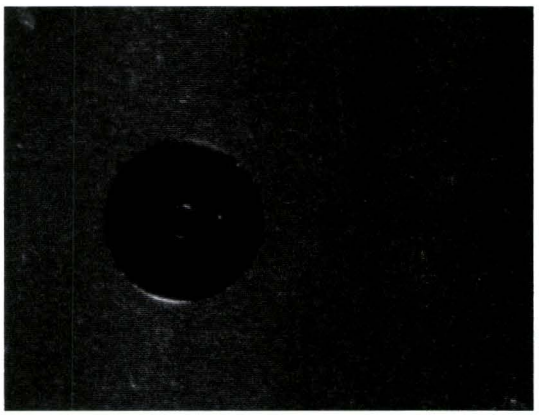

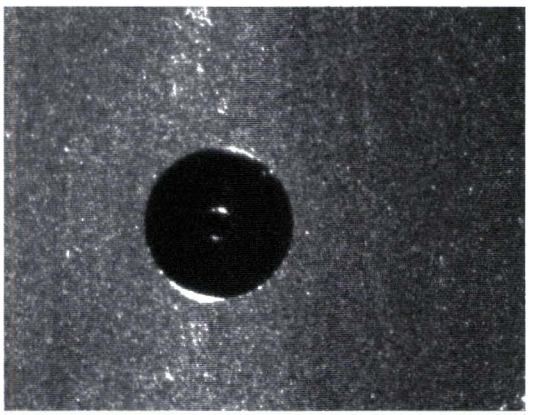

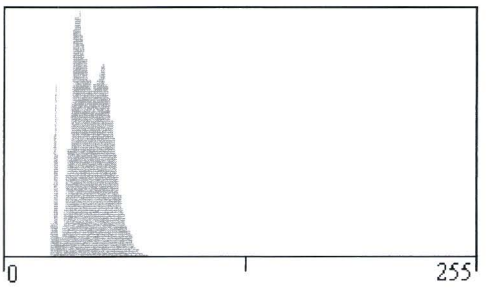

Figure B1a: Sony SSC-C370, shutter 1/50 seconds (minimal)

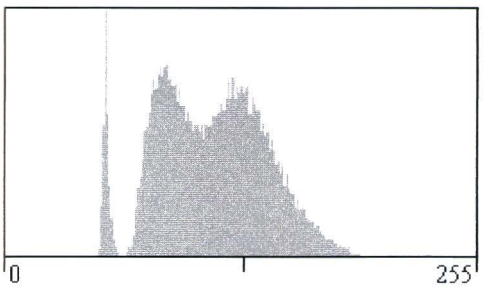

Figure B1b: Watec LCL 902K, shutter 1/50 seconds (minimal)

The camera will be used to track the motion of particles in the ink. To distinguish the light scattered from moving particles, from the light scattered by the structure of the nozzle plate, a background correction is performed by subtraction of two sequent frames.

Figure B2 and B3 show the pixel values along a line in the difference images. A moving object is visible as a spike in the pixel value.

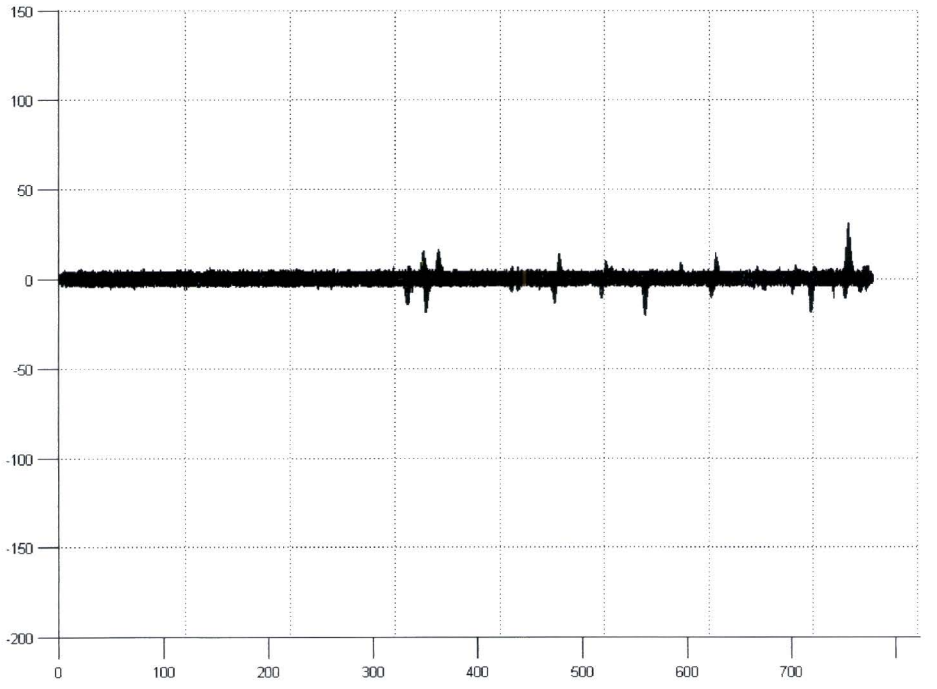

Figure B2: Pixel value along line (Sony camera)

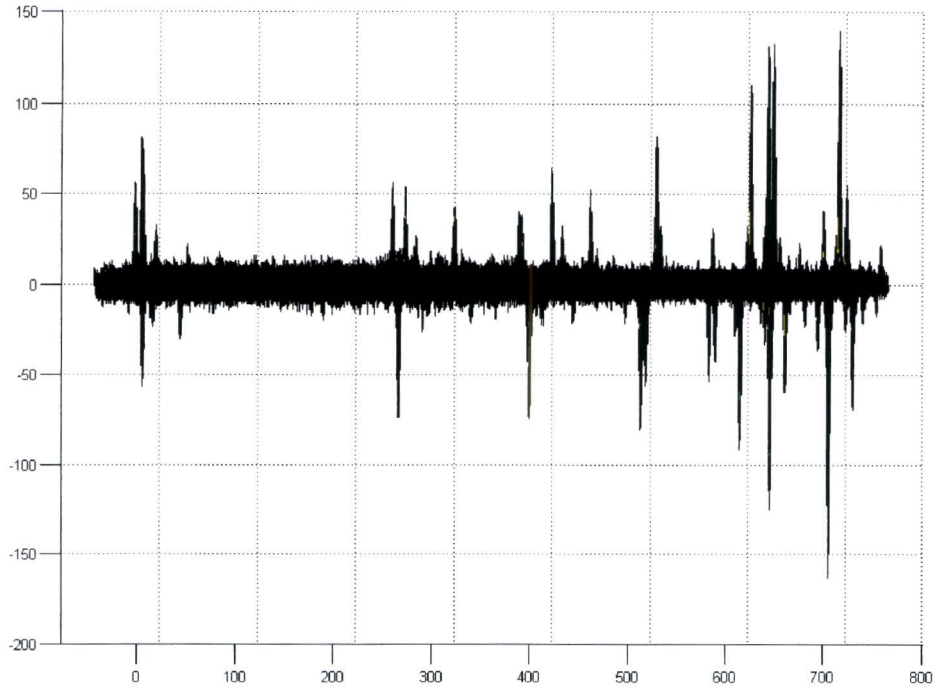

Figure B3: Pixel Value along line (Watec camera)

From these figures can be concluded that the signal/noise ratio of the image obtained by the Sony camera is much smaller then the signal/noise ratio of the image obtained by the Watec camera.

B2. Conclusion

As expected, the Watec camera is much more sensitive at low light conditions then the Sony camera. This can be concluded from the specifications and is supported by the measurements.

From the measurements can be concluded that the signal/noise ratio of the Watec camera is much higher then the signal/noise ratio of the Sony Camera. A high signal/noise ratio makes it easier to distinguish, since choosing a threshold performs the detection of a particle.

It can be concluded that using the Watec camera performing measurements and tracking particles will be much more accurate.